Finite Element Study on the Flexural Behaviour and Edge-Stiffening Effect of Cold-Formed Steel C-Channel Beams with Elongated Web Holes

A thesis

submitted in partial fulfilment

of the requirements for the degree

of

Master of Civil Engineering

at

The University of Waikato

By

Junhong Lei

THE UNIVERSITY OF
WAIKATO
Te Whare Wānanga o Waikato
NEW ZEALAND

2026

Acknowledgements

This research was completed under the supervision of Dr Arthur Fang. His careful guidance, constructive feedback and rigorous academic standards greatly improved the quality of this thesis. His advice on finite element modelling, interpretation of the numerical results and thesis preparation strengthened both my research skills and academic writing. I am sincerely grateful for his time, patience and encouragement throughout my master's study.

I would also like to express my sincere gratitude to Ro Ma for his generous support and guidance in finite element analysis. His technical advice and practical experience helped me resolve many difficulties encountered during the development and analysis of the FE models. His assistance made a valuable contribution to the completion of this research.

I am deeply grateful to my friends for their companionship, encouragement and support throughout my master's study. Their presence made this challenging period more enjoyable and gave me the confidence to continue during difficult moments.

My sincere thanks go to my parents and family for their unconditional support, understanding and encouragement. Although we lived in different countries, their concern for my life and studies never diminished. Their emotional and financial support enabled me to complete my master's degree and gave me the courage to face the challenges of studying abroad.

Finally, I would like to thank everyone who contributed to this research or supported me during my studies but could not be mentioned individually. Their kindness and assistance are sincerely appreciated.

Table of Contents

List of Figures

List of Tables

ABSTRACT

Cold-formed steel (CFS) channel beams are commonly provided with web openings to allow building services to pass through the member. In practice, larger openings are often preferred because they provide more space for services. However, increasing the opening size may reduce the flexural resistance of the beam, especially when elongated web holes are used. This thesis investigates the flexural behaviour of CFS channel beams with elongated web holes under four-point bending. The main aim is to examine whether larger web openings can be introduced while maintaining an acceptable level of moment capacity. The effectiveness of edge stiffening around elongated web holes is also evaluated.

A nonlinear elasto-plastic finite element model was developed in Abaqus. The modelling approach was first validated against published experimental and numerical results for CFS channel beams with web holes. After validation, a parametric study including 282 finite element models was carried out. Two section sizes, C240 and C290, were considered. Their no-hole moment capacities were 13.591 kN·m and 20.058 kN·m, respectively. The main parameters included hole radius, elongated-hole aspect ratio, number of holes, clear spacing between adjacent holes, edge stiffening, and lip angle. Three hole radii of 70, 75, and 80 mm were examined. The elongated-hole aspect ratio was varied from 1.25 to 2.00. One-hole, two-hole, and three-hole arrangements were included, with clear spacings of 50 and 100 mm for the multi-hole models. For the edge-stiffened models, the stiffener depth and fillet radius were kept as 13 mm and 4 mm, respectively.

The results show that increasing the web opening area generally reduced the moment capacity of the unstiffened-hole beams. For the more severe practical cases, the strength retention ratio decreased to about 0.78–0.85. By contrast, edge stiffening was able to recover a considerable part of the lost strength. The maximum stiffening efficiency obtained in this study was approximately 26.6%. In several edge-stiffened three-hole models, the strength retention ratio remained above 0.85 even when the opening ratio exceeded 12%. The lip-angle study also showed that the flange-lip inclination can affect the flexural response. Among the investigated C290 EH1-HS80-ab15 models, the 60° lip-angle model gave the highest moment capacity. Overall, the results indicate that elongated web holes can be used more efficiently when suitable edge stiffening and geometric configurations are adopted.

Keywords: Cold-formed steel; channel beam; elongated web hole; edge-stiffened hole; finite element analysis; moment capacity

1. Introduction

1.1. Background

Cold-formed steel (CFS) C-channel beams are widely used in light-gauge steel construction. They are lightweight, economical, and relatively straightforward to manufacture. These members are also suitable for prefabricated construction. One example is the floor joist system developed by Howick Ltd. [1].

In practice, electrical cables, water pipes, and other building services often need to pass through floor and wall members. Web openings are therefore commonly pre-punched in CFS channels during manufacturing. This provides a convenient route for services and can reduce the need for additional work on site.

However, removing material from the web also changes the structural response of the member. The opening interrupts the normal stress path and reduces the stiffness of the surrounding web. Under bending, stresses may become concentrated near the hole edge. Local or distortional buckling may also develop around the opening.

Previous studies have examined the flexural behaviour of CFS channel beams without web holes, including local buckling, distortional buckling, and interaction between these modes [2-6]. The introduction of web openings makes the response more complicated. Depending on the size, shape, and position of the opening, the net section, load-transfer path, and governing buckling mode may all change.

Chandramohan et al. (2025) investigated the flexural behaviour of cold-formed steel channel beams with unstiffened and edge-stiffened elongated web holes. The main parameters considered in their finite element parametric study included the web-hole stiffening condition, elongated-hole dimensions, beam length, and channel-section geometry. The moment capacity and associated buckling/failure modes were used as the main response measures.[34-37]

1.2. Literature Review

A number of studies have investigated CFS members with unstiffened web holes. Zhao et al. [7] tested CFS channel beams with unstiffened web holes and discussed the limitations of existing Direct Strength Method predictions. Moen and Schafer [8-10] also studied cold-formed steel members with perforations and proposed design procedures that account for the effects of web holes. Yu et al. [11,12] subsequently investigated the distortional buckling behaviour of perforated CFS beams. Kulatunga and co-workers [13,14] examined CFS columns containing circular and elongated perforations. These studies demonstrated that web openings can alter the strength, stiffness, and governing buckling behaviour of cold-formed steel members.

Edge-stiffened web holes have been investigated as a method of reducing the adverse effects caused by removing web material. Chen et al. [15,16] examined CFS channel sections with edge-stiffened web openings under compression and found that stiffening the hole boundary could improve the load-carrying capacity. Yu [17] reported through numerical analysis that appropriately proportioned edge stiffeners could increase the moment capacity of CFS flexural members. Uzzaman et al. [18,19] also showed that edge-stiffened web openings could improve the web crippling resistance of CFS channel sections. These studies mainly concerned circular openings but established that local stiffening around a hole can recover part of the capacity lost through web perforation.

The treatment of web openings in current design standards remains limited. AISI S100-16 [20] and AS/NZS 4600:2018 [21] do not provide direct design rules for CFS C-channel beams with edge-stiffened elongated web holes. The design procedures developed by Moen and Schafer [8-10] are useful for members with conventional unstiffened perforations, but their direct application to elongated edge-stiffened openings is limited.

Early research by LaBoube et al. [33] examined C-section beams containing web openings and developed design recommendations covering bending, shear, web crippling, and combined loading conditions. This work provided an important foundation for understanding the structural effects of service openings, including elongated openings. However, the opening boundaries considered in that study were not representative of the more recent elongated edge-stiffened configurations.

More recent studies have examined elongated openings more directly. Chandramohan et al. [34] investigated the moment capacity and flexural behaviour of CFS channel beams containing elongated edge-stiffened and unstiffened web holes. Their numerical parametric study included 2160 FE models. On average, the elongated edge-stiffened models achieved a moment capacity approximately 9 percent higher than that of the corresponding unstiffened models. Modified Direct Strength Method equations were also proposed for both opening types.

The behaviour of elongated edge-stiffened and unstiffened openings under other loading conditions has also been investigated. Chandramohan et al. [35] studied their shear behaviour through a parametric investigation comprising 2124 FE analyses and proposed shear reduction factors and modified Direct Strength Method equations. Chandramohan et al. [36] examined the same general opening types under axial compression using 990 FE results and proposed capacity equations based on the Effective Width Method and Direct Strength Method.

For unstiffened elongated openings, Pham et al. [37] investigated cold-formed channels containing rectangular and slotted web openings under shear. Their nonlinear FE models were calibrated against previous experimental results and used to study elastic shear buckling, post-buckling behaviour, and the applicability of existing design methods. The study showed that elongated opening geometry can substantially influence the shear behaviour and failure mechanism of perforated channels.

These studies confirm that elongated web openings have been examined under bending, shear, and compression. However, much of the available evidence for elongated edge-stiffened openings is numerical, while direct experimental evidence under flexural loading remains limited. The interaction between practical opening parameters and their influence on peak capacity, post-peak response, and local deformation also requires further assessment for specific channel geometries.

The present study therefore evaluates selected C240 and C290 C-channel beams with elongated unstiffened and edge-stiffened web holes under bending. The investigated parameters include hole radius, opening aspect ratio, number of openings, clear spacing, and lip angle. The study does not claim that elongated edge-stiffened holes have not previously been investigated. Instead, it provides a focused assessment of selected practical configurations and examines both peak moment capacity and post-peak response within the adopted FE model range.

In summary, previous studies have confirmed the importance of elongated web openings and edge stiffening in CFS channel members. However, direct experimental evidence for elongated edge-stiffened openings under bending remains limited, and most available studies focus mainly on ultimate capacity rather than post-peak behaviour. The combined influence of practical opening parameters, including hole radius, aspect ratio, number of openings, clear spacing and lip angle, also requires further assessment for specific C-channel geometries. Therefore, the present study provides a focused FE investigation of selected C240 and C290 channel beams to examine peak moment capacity, post-peak response and local deformation behaviour within the adopted model range.

1.3. Research Aim and Scope

The main purpose is not only to find the strongest model, but also to find a practical balance between opening size and strength loss. In real construction, a larger opening is useful only when the beam can still keep enough bending resistance. Therefore, this study compares the ultimate moment capacity Mu, the displacement at the peak moment δu, the strength retention ratio Mu/M_0, the opening ratio ρ, and the stiffening efficiency η. The plain beam without web holes is used as the reference model for each section, and its ultimate moment capacity is defined as M_0.

The parametric study includes 282 finite element models. The main parameters are hole type, number of holes, hole radius, elongated-hole aspect ratio, clear spacing between holes, and lip angle. Three hole radii are considered: 70 mm, 75 mm, and 80 mm. The aspect ratios of the elongated holes are 1.25, 1.50, 1.75, and 2.00. For beams with two or three holes, clear spacings of 50 mm and 100 mm are included. In addition, selected UH1 and EH1 models are used to study the effect of lip angles of 20°, 45°, 60°, 75°, and 90°.

1.4. Contribution of this study

A focused FE parametric study was conducted on selected practical elongated-hole configurations based on the method of Chen et al. In the first stage, the reference FE models for CFS channel beams with plain webs, unstiffened circular web holes, and edge-stiffened circular web holes were reproduced. This reproduction was carried out to check the modelling procedure, including material modelling, boundary conditions, contact definitions, mesh strategy, initial imperfections, and four-point bending loading. The reproduced models were then compared with the reference numerical results.

After the reproduction and validation stage, the model was extended to study elongated web holes. This part forms the main contribution of the present thesis. Unlike the reference study, which mainly considered circular web holes, the present study focuses on elongated web holes with different hole sizes and arrangements. The parameters investigated include hole radius, elongated-hole aspect ratio, number of holes, clear spacing between adjacent holes, edge stiffening, and lip angle.

A total of 282 finite element models were analysed in this study. These models include no-hole beams, unstiffened elongated web-hole beams, and edge-stiffened elongated web-hole beams for both C240 and C290 sections. The study also considers three hole radii of 70 mm, 75 mm, and 80 mm, four elongated-hole aspect ratios of 1.25, 1.50, 1.75, and 2.00, and one-hole, two-hole, and three-hole arrangements. For the multi-hole models, clear spacings of 50 mm and 100 mm were included. In addition, selected single-hole models were used to study the effect of lip angle.

The main contribution of this thesis is therefore not the original development of a new FE modelling method. Instead, the contribution lies in applying a validated modelling approach to a wider group of elongated web-hole configurations. The study provides numerical evidence on how elongated-hole geometry affects moment capacity, strength retention, opening ratio, and stiffening efficiency. It also examines whether edge stiffening can help larger web openings maintain an acceptable level of flexural resistance.

In summary, the contributions of this study are as follows:

1. The FE modelling approach reported by Chen et al. [22] was reproduced and checked against the reference results.

2. The validated modelling approach was extended from circular web holes to elongated web holes.

3. A parametric study with 282 FE models was carried out for C240 and C290 channel beams.

4. The effects of hole radius, elongated-hole aspect ratio, clear spacing, number of holes, edge stiffening, and lip angle were investigated.

5. The study evaluated the balance between increasing the web opening area and maintaining the moment capacity of CFS C-channel beams.

6. The results provide a numerical basis for further research on edge-stiffened elongated web holes, including future experimental work and possible design recommendations.

1.5. Thesis Outline

This thesis is organised into five chapters.

Chapter 1 introduces the background of CFS C-channel beams with web openings. It reviews previous studies on plain CFS beams, beams with unstiffened web holes, and beams with edge-stiffened web holes. The research gap, aim, and scope of the present study are then described.

Chapter 2 presents the reference study and the finite element modelling method used in this research. The geometry of the C240 and C290 sections, material properties, loading arrangement, boundary conditions, mesh strategy, and output quantities are described. The plain beam models are also introduced because they provide the reference moment capacity M_0.

Chapter 3 describes the parametric study. The model naming system, hole geometry, hole spacing, edge stiffening details, and lip angle cases are explained. This chapter also defines the main evaluation indices, including opening ratio ρ, strength retention ratio Mu/M_0, and stiffening efficiency η.

Chapter 4 presents and discusses the numerical results. Moment-displacement curves, ultimate moment capacities, strength retention ratios, opening ratios, and stiffening efficiencies are compared. The effects of hole radius, aspect ratio, clear spacing, number of holes, edge stiffening, and lip angle are discussed one by one.

Chapter 5 summarises the main findings of the study. It gives the main conclusions on which hole configurations are more efficient and discusses the limitations of the present work. Suggestions for future research are also provided.

2. Finite Element Modelling

2.1. General

In this study, ABAQUS 2024 [29] was used to develop the finite element models. The models were used to study the moment capacity of CFS channel beams. Three types of beams were considered. These were beams without web holes, beams with unstiffened web holes, and beams with edge-stiffened web holes.

Before carrying out the main parametric study, the numerical models from Chen et al. [22] were first reproduced. This step was useful because it allowed the modelling procedure to be checked against an existing study. The reproduced models followed the same general modelling assumptions as the reference work. These included the measured section dimensions, initial geometric imperfections, and material properties from coupon tests. The material properties used in the reproduced models are listed in Table 2.1.

The channel beams were modelled using shell elements. The load transfer blocks were also included in the model so that the four-point bending condition could be represented properly. During the reproduction stage, the mesh arrangement was checked carefully. Fig. 2.1 shows a comparison between the mesh reported by Chen et al. [22] and the mesh used in the present reproduced model. The mesh was refined around the web opening and near the rounded corners. This was done because local deformation and stress concentration are more likely to occur in these regions.

After the model was generated, the stress distribution was also examined. Fig. 2.2 shows the Von Mises stress contour of the reproduced C290-EH1 circular-hole model under four-point bending. The stress pattern shows that the web opening and the bending region are the main areas of stress concentration. This behaviour is reasonable for a CFS channel beam with a web hole.

The reproduced models were then checked against the reference results. The comparison included the ultimate moment capacity, the moment-deflection response, and the failure behaviour. This validation was necessary before the model was used for further parametric work. After the model had been checked, it was extended to the elongated-hole models used in this study. These later models included different hole radii, aspect ratios, hole spacings, hole numbers, edge-stiffening conditions, and lip angles.

2.2. Material model

No coupon tests were conducted in the present study. Since the FE models were developed to reproduce the experimental and numerical results reported by Chen et al. [22], the material properties used in the present models were adopted from their coupon tensile test data. This ensured that the reproduced FE models used material input data consistent with the reference study.

The CFS channel beams were modelled using an elastic-plastic material model. Both the flat and corner regions of the C240 and C290 channel sections were considered separately, following the material characterisation reported by Chen et al. [22]. This distinction was necessary because the cold-forming process causes plastic deformation and strain hardening in the corner regions. As a result, the corner material generally has higher yield and ultimate stresses than the flat material. The adopted material properties are listed in Table 2.1.

Table 2.1

Material properties adopted from Chen et al. [22] for the finite element models

Section / Region	Thickness (mm)	Young's modulus (MPa)	Yield stress (MPa)	Ultimate stress (MPa)	Source
C240 flat region	1.83	192,057	332.8	420.5	Chen et al. [22]
C240 corner region	1.82	210,052	363.4	431.8	Chen et al. [22]
C290 flat region	2.11	196,136	330.7	415.8	Chen et al. [22]
C290 corner region	2.13	211,003	362.2	430.5	Chen et al. [22]

The nonlinear material response was defined in Abaqus using true stress and logarithmic plastic strain. Therefore, the engineering stress-strain data reported by Chen et al. [22] were converted before being input into the FE model. The engineering stress and engineering strain were converted into true stress and true strain using Eqs. (2.1) and (2.2):

$$\sigma_{true} = \sigma(1 + \varepsilon) \quad (2.1)$$

$$\sigma_{true(pl)} = \ln(1 + \varepsilon) - \sigma_{true}/E \quad (2.2)$$

The logarithmic plastic strain was then obtained by subtracting the elastic strain from the true strain:

$$\sigma_{true(pl)} = \frac{\varepsilon_{true} - \sigma_{true}}{E} \quad (2.3)$$

where σ and ε are the engineering stress and engineering strain, respectively; σ_{true} and ε_{true} are the true stress and true strain; $\varepsilon_{true(pl)}$ is the logarithmic plastic strain used in Abaqus; and E is Young's modulus.

The converted true stress and logarithmic plastic strain data were used to define the plastic material behaviour. The material curve was defined using the available coupon test data up to the ultimate stress reported by Chen et al. [22]. No artificial post-ultimate extension was introduced, because the bending response of the channel beams was governed mainly by local buckling, stress redistribution and deformation around the web openings rather than by material fracture.

The loading and support blocks were used only to transfer the applied load and boundary conditions to the channel beam. These blocks were assigned elastic material properties with a Young's modulus of 200 GPa. Their material response was not intended to represent the behaviour of the CFS channel beam, and their deformation was not considered part of the structural response investigated in this study.

To ensure consistent interpretation of the numerical results, the main response indices used in the present study are defined in Table 2.2. These indices were used to compare the bending resistance of different web-opening configurations and to evaluate the effect of edge stiffeners.

Table 2.2

Notation used for response indices.

Symbol	Definition	Formula
Pmax	Maximum total vertical reaction force	-
a	Shear span between support and nearest loading point	-
Mu	Ultimate bending moment	Mu = Pmax a / 2
M0	Gross-section moment capacity of the corresponding channel beam without web openings	M0 = fy×Z
Mu/M0	Normalised moment capacity	Mu/M0

Symbol	Definition	Formula
rho	Web opening ratio	rho = d / hw
eta	Stiffening efficiency	eta = $\frac{M_{u(EH)}}{M_{u(UH)}}$

2.3. Element type and mesh size

S4R shell elements were used to model the CFS channel beams. These are four-node quadrilateral shell elements with reduced integration and six degrees of freedom per node.

No independent mesh sensitivity study was conducted in the present work. Instead, the mesh arrangement was adopted from Chen et al. [22], whose mesh sensitivity analysis indicated that a nominal mesh size of 5 mm × 5 mm was suitable for CFS channel beams with and without web openings. A mesh size of 10 mm × 10 mm was adopted for the load-transfer blocks. Following the reference model, local mesh refinement was applied around the web openings, with finer elements used near the curved edges. Figure 1 compares the reference mesh with the mesh reproduced in the present study.

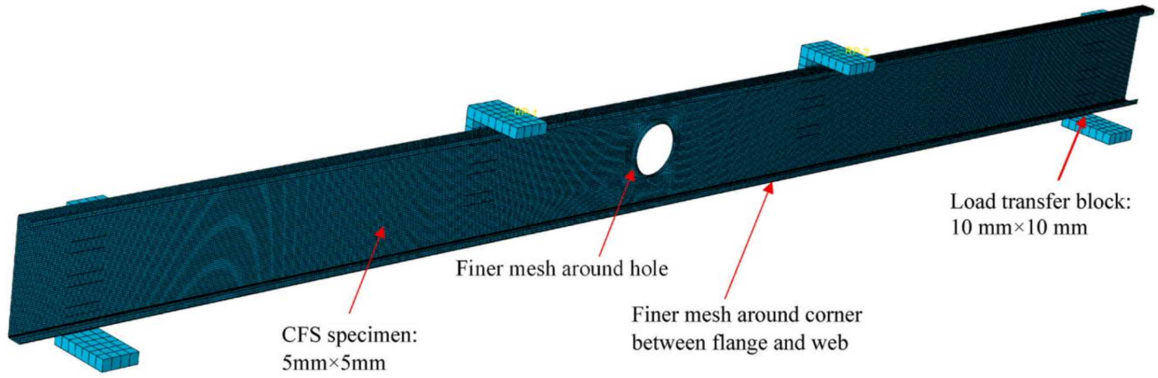

(a) Reference finite element mesh reported by Chen et al. [22]

(b) Reproduced finite element mesh used in the present study

Figure 1 Comparison of the finite element mesh reported by Chen et al. [22] and the reproduced mesh used in the present study.

2.4. Boundary conditions and loading procedure

The boundary conditions and loading arrangement used in the FE model are shown in Fig 2. The Abaqus global coordinate system was defined such that the beam longitudinal direction was the global Z direction, the vertical loading direction was the global Y direction, and the out-of-plane direction was the global X direction. Therefore, U1, U2 and U3 represent the translational degrees of freedom in the X, Y and Z directions, respectively.

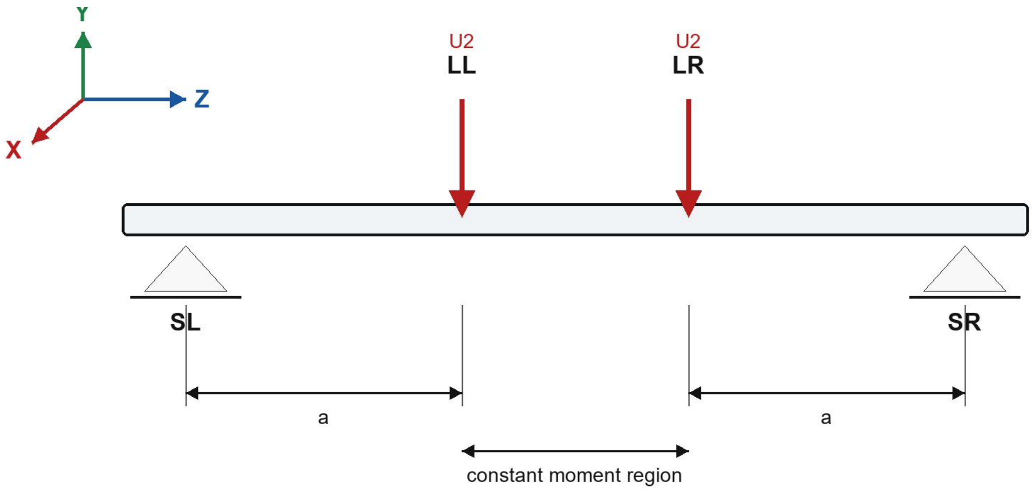

Figure 2 Boundary condition schematic of the four-point bending FE model.

The four-point bending setup was simulated using two support points and two loading points. The support points were denoted as SL and SR, while the loading points were denoted as LL and LR. Rigid loading and support blocks were used to transfer the load and support reactions to the channel beam. Each block was assigned a reference point, and the corresponding block surfaces were tied to the beam contact regions. The boundary conditions and loading were applied at the reference points of these rigid blocks.

The boundary conditions applied in the nonlinear static analysis are summarised in Table 2.2. At the two loading points, LL and LR, the out-of-plane displacement U1 and rotation about the beam longitudinal axis UR3 were restrained. The vertical displacement U2 was then imposed at both loading points to simulate displacement-controlled loading. A downward displacement of 30 mm was applied in the negative global Y direction. At the support points, the vertical displacement U2 was restrained. The out-of-plane displacement U1 and rotation UR3 were also restrained to prevent lateral movement and rigid body rotation. In addition, the longitudinal displacement U3 was restrained at support SR to prevent rigid body translation along the beam length, while it was released at SL to avoid over-constraining the model.

Table 2.3

Boundary conditions applied at the support and loading reference points.

Reference point	Location	Restrained degrees of freedom	Applied displacement
LL	Loading point	U1, UR3	U2 = -30 mm
LR	Loading point	U1, UR3	U2 = -30 mm
SL	Support point	U1, U2, UR3	-
SR	Support point	U1, U2, U3, UR3	-

The ultimate moment was calculated from the total vertical reaction force obtained from the two supports. For the four-point bending configuration, the maximum bending moment in the constant moment region was calculated as:

$$M_u = \frac{P_{\max}}{2} a$$

where Pmax is the total applied vertical load, taken as the sum of the vertical reaction forces at the two supports, and a is the shear span between the support and the nearest loading point. In the present model, the shear span was 1200 mm. Therefore, when Pmax is expressed in N, the ultimate moment in kNm was calculated as:

$$a = 1200 \text{ mm}$$

Therefore, when P_{max} is expressed in N, the ultimate moment in kNm was calculated as:

$$M_u = \frac{P_{\max} \times 1200}{2 \times 10^6}$$

This calculation was used consistently for the validation model and the imperfection sensitivity study.

2.5. Modelling of initial geometric imperfections

Initial geometric imperfections were considered in the FE modelling because cold-formed steel channel beams are sensitive to small geometric deviations. This is particularly important for thin-walled members, where local plate deformation and overall bending may develop before the peak moment is reached. Therefore, representative local and global geometric imperfections were introduced into the channel beam models to obtain a more realistic nonlinear bending response.

The imperfection amplitudes used in this study were adopted from the measured values reported by Chen et al. [22]. In their experimental programme, the initial imperfections of the test specimens were measured using a laser scanner before the four-point bending tests. The measured imperfections included local, distortional and global components. For the representative C290-EH1 model, the measured local, distortional and global imperfection amplitudes were 0.59 mm, 1.02 mm and 1.50 mm, respectively. These measured values were used as the basis for scaling the selected imperfection shapes in the present FE models.

Although the measured distortional imperfection amplitude is reported above for completeness, distortional imperfections were not introduced as a separate imperfection component in the main FE models. This treatment follows the observation reported by Chen et al. [15], where distortional imperfections had only a limited influence on the predicted failure load and deformation pattern of CFS channel beams with edge-stiffened web openings. Therefore, the imperfection modelling in the present study focused on local and global imperfections, which are more directly associated with local plate deformation around the web opening and the overall bending deformation of the beam.

The imperfection shapes were obtained from eigenvalue buckling analyses in Abaqus 2024 [29]. For the global imperfection shape, the full-thickness C290-EH1 model was used. The original shell thickness of the CFS channel section was 2.11 mm. The first eigenmode showed an overall bending deformation of the beam and was therefore selected as the global imperfection mode. This mode was scaled to the measured global imperfection amplitude of 1.50 mm for the C290-EH1 model.

For the local imperfection shape, a reduced-thickness buckling model was used to obtain a clearer local plate buckling mode. In this auxiliary buckling analysis, the CFS shell thickness was temporarily reduced from 2.11 mm to 1.05 mm, approximately 0.5 times the original thickness. This thickness reduction was used only for extracting the local eigenmode shape and was not used in the subsequent nonlinear static bending analysis. The first eigenmode of the reduced-thickness model showed local plate deformation around the loading region and the web opening, and was therefore selected as the local imperfection mode. This mode was scaled to the measured local imperfection amplitude of 0.59 mm for the C290-EH1 model.

The selected global and local buckling modes used for imperfection modelling are shown in Fig 3.

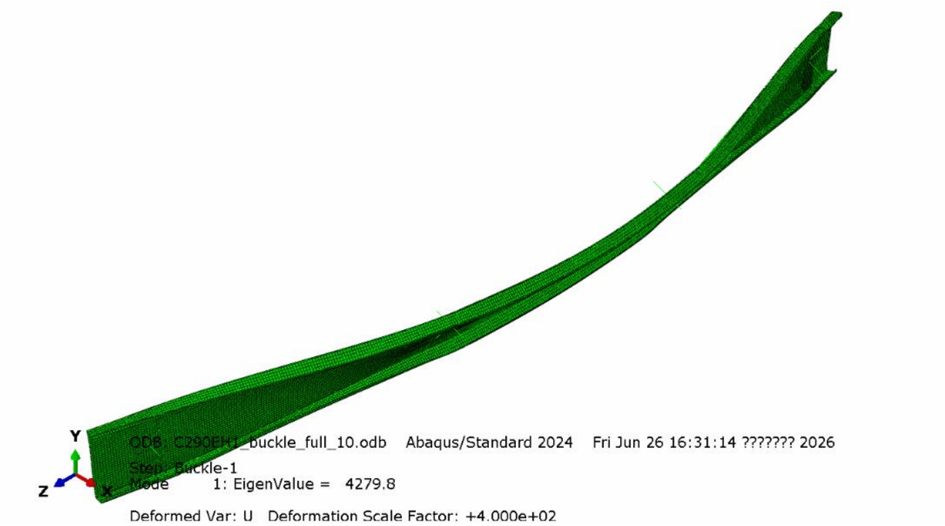

(a) Global mode (full-thickness model, Mode 1)

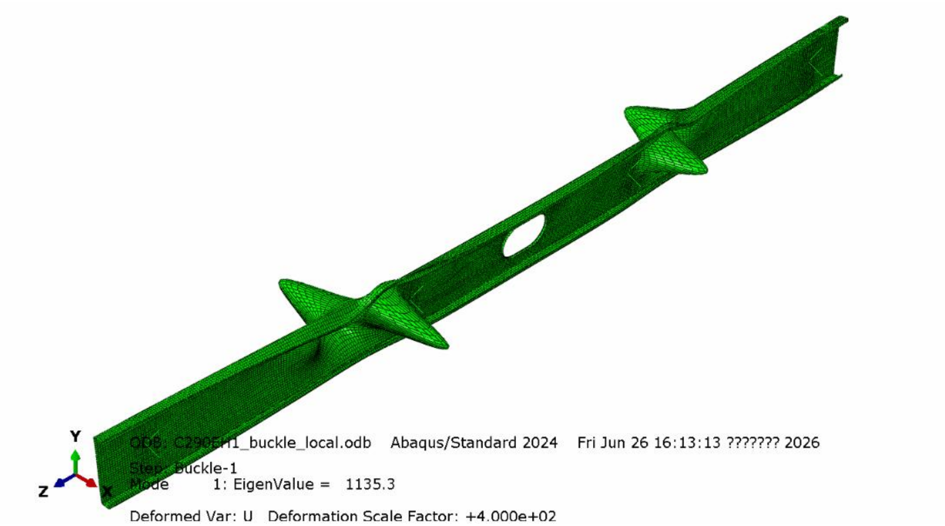

(b) Local mode (reduced-thickness model, Mode 1)

Figure 3 Selected buckling modes used for imperfection modelling: (a) global mode obtained from the full-thickness model; (b) local mode obtained from the reduced-thickness model.

Selected buckling modes used for imperfection modelling: (a) global mode obtained from the full-thickness model; (b) local mode obtained from the reduced-thickness model.

The selected imperfection modes were introduced into the nonlinear static models using the Abaqus *IMPERFECTION keyword. For the combined local-global imperfection case, the full-thickness buckling model was used so that both imperfection components could be defined from the same buckling results file. In this model, Mode 1 represented the global bending mode and Mode 3 represented a local plate buckling mode. These two modes were scaled to 1.50 mm and 0.59 mm, respectively.

For the two-hole models in the parametric study, no direct counterpart was available in the reference experimental programme. Therefore, the imperfection amplitudes of the corresponding three-hole specimens with the same section size and hole type were adopted. This assumption was considered reasonable because the purpose of the imperfection modelling was to introduce representative initial geometric deviations rather than to reproduce specimen-specific measured imperfections for each parametric model.

To examine whether the adopted imperfection treatment had a significant influence on the predicted bending resistance, an imperfection sensitivity study was carried out using the representative C290-EH1 model. Four cases were compared: the nominal model without initial imperfections, a model with global imperfection only, a model with local imperfection only, and a model with combined local and global imperfections. The results are summarised in Table 2.2.

Table 2.4

Imperfection sensitivity study for the representative C290-EH1 model.

Case	Imperfection type	Imperfection source	Ultimate moment, Mu (kNm)	Difference from nominal model
Case 0	No imperfection	-	20.246	0.00%
Case 1	Global only	Mode 1, 1.50 mm	20.457	+1.04%
Case 2	Local only	Mode 1, 0.59 mm	19.904	-1.69%
Case 3	Local + global	Mode 1, 1.50 mm + Mode 3, 0.59 mm	19.505	-3.66%

The sensitivity study shows that the inclusion of local and global geometric imperfections changed the predicted ultimate moment by less than 4%. The largest reduction was obtained for the combined local-global imperfection case, where the ultimate moment decreased by 3.66% compared with the nominal model. This indicates that the predicted bending resistance of the representative model was not highly sensitive to the selected imperfection assumptions. Therefore, the adopted imperfection modelling approach was considered reasonable for the present FE study. Since previous studies reported a limited influence of distortional imperfections and the present local-global sensitivity study produced only a small variation in ultimate moment, distortional imperfections were not included as a separate imperfection component in the subsequent parametric models.

2.6. Analysis methods

Two analysis procedures were used in the FE modelling. First, elastic buckling analysis was carried out to obtain the eigenvectors required for modelling the initial geometric imperfections. After that, the nonlinear bending response was calculated using a static general analysis step in ABAQUS 2024 [29].

The static analysis was performed with geometric nonlinearity enabled. This was necessary because the CFS channel beams experienced local deformation and post-buckling behaviour during four-point bending. Automatic stabilization was also used to improve convergence during the nonlinear response. In the representative model checked in this study, the stabilization factor was 0.0002. No mass scaling was used.

The loading was applied by imposing a vertical displacement of 30 mm at the loading reference points. The total step time was 1.0. Since a static procedure was used, this step time should be understood as pseudo-time for load incrementation, rather than real dynamic time. Therefore, the nominal loading rate was 30 mm per unit pseudo-time. The main analysis settings and the energy check for the representative model are summarised in Table 2.3.

Table 2.5

Quasi-static check and analysis settings for the representative FE model.

Model	Analysis procedure	Step time	Applied displacement	Nominal loading rate	Max ALLKE/ALLIE	Mass scaling	Stabilization / damping
C290-EH1-HS75-ab15-s50 refined mesh	Static general, NLGEOM	1.0 pseudo-time	30 mm	30 mm per unit pseudo-time	0.000%	Not used	Automatic stabilization, factor = 0.0002

Although the analysis was not an implicit dynamic analysis, the kinetic energy was still checked to confirm that no inertial effect was introduced. For the representative refined model, the maximum ALLKE/ALLIE ratio was 0.000%, as shown in Table 2.3. This shows that the kinetic energy was negligible compared with the internal energy. Therefore, the calculated response can be treated as a quasi-static bending response.

A typical stress distribution obtained from the reproduced model is shown in Fig 4. The figure presents the von Mises stress contour of the C290-EH1 circular-hole model under four-point bending. Stress concentration can be observed around the web opening and within the constant moment region. This response is consistent with the expected behaviour of a CFS channel beam with a web hole.

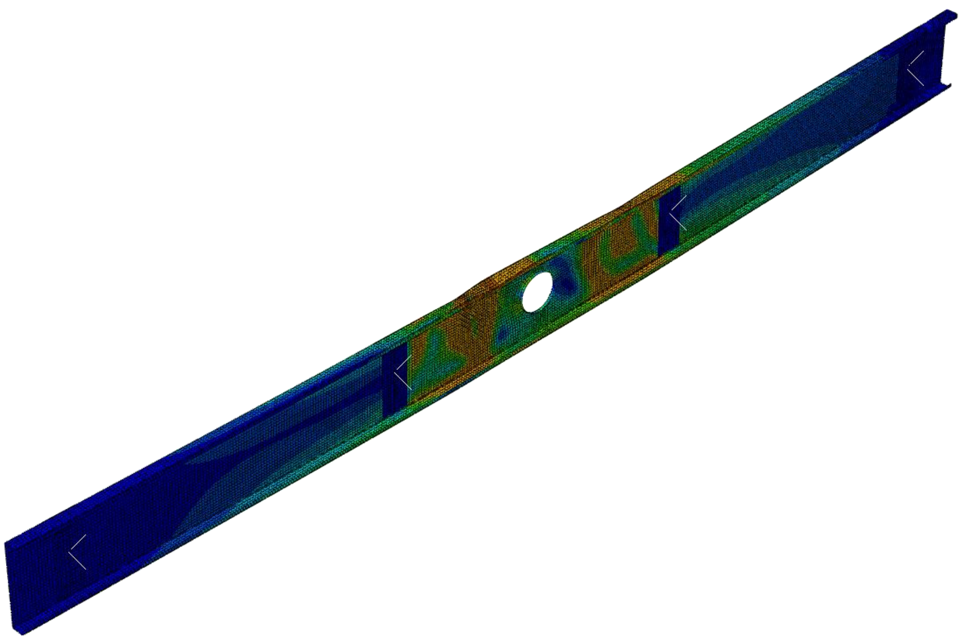

Figure 4 Von Mises stress contour of the reproduced C290-EH1 circular-hole model under four-point bending.

2.7. Validation of the FE model

The FE model was checked against the numerical results reported by Chen et al. [22]. In their study, four-point bending tests were carried out on CFS channel beams with plain webs, unstiffened web holes, and edge-stiffened web holes. The same modelling logic was followed in the present study. Therefore, the reproduced FE results were compared with the corresponding reference data for both the C240 and C290 sections.

Before comparing the ultimate moment capacities, the no-hole baseline models were examined first. The moment-deflection curves of the reproduced C240-NH and C290-NH models were compared with the NH curves reported by Chen et al. [22]. As shown in Fig 5, the reproduced curves show similar initial stiffness, peak moment level, and post-peak softening behaviour to the reference curves. The peak moments of the reproduced C240-NH and C290-NH models are 13.591 kN·m and 20.058 kN·m, respectively. This comparison gives a first check of the baseline models. After that, the validation was extended to the models with web holes.

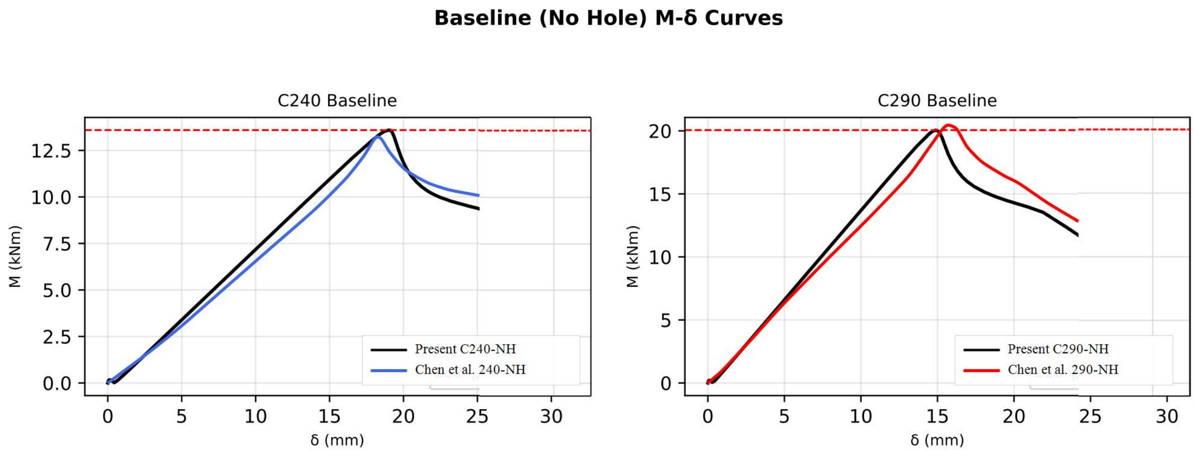

Figure 5 Comparison of baseline moment-deflection curves between the reproduced NH models and the reference NH curves reported by Chen et al. [22].

Table 2.6

Comparison of moment capacity between the reference FEA and the reproduced FEA.

Specimen ID	Moment capacity obtained from reference FEA, $M_{Ref,FEA}$ (kN·m)	Moment capacity obtained from reproduced FEA, $M_{Present,FEA}$ (kN·m)	Comparison $M_{Present,FEA}$ / $M_{Ref,FEA}$
Section 240			
240-L4000-NH	13.20	13.591	1.030

240-L4000-EH1	13.40	13.675	1.021
240-L4000-EH3	13.80	13.577	0.984
240-L4000-UH1	12.20	11.706	0.960
240-L4000-UH3	11.70	11.896	1.017
Section 290			
290-L4000-NH	20.30	20.058	0.988
290-L4000-EH1	19.65	20.109	1.024
290-L4000-EH3	20.24	21.090	1.042
290-L4000-UH1	18.60	18.620	1.001
290-L4000-UH3	18.10	17.600	0.972

The reproduced FE moment capacities were compared with the corresponding reference FE results reported by Chen et al. [22]. The comparison is presented in Table 2.6. The comparison ratios range from 0.960 to 1.042, which indicates that the reproduced models provide a reasonable agreement with the reference numerical results.

Validation of Present FE Results against Reference Data

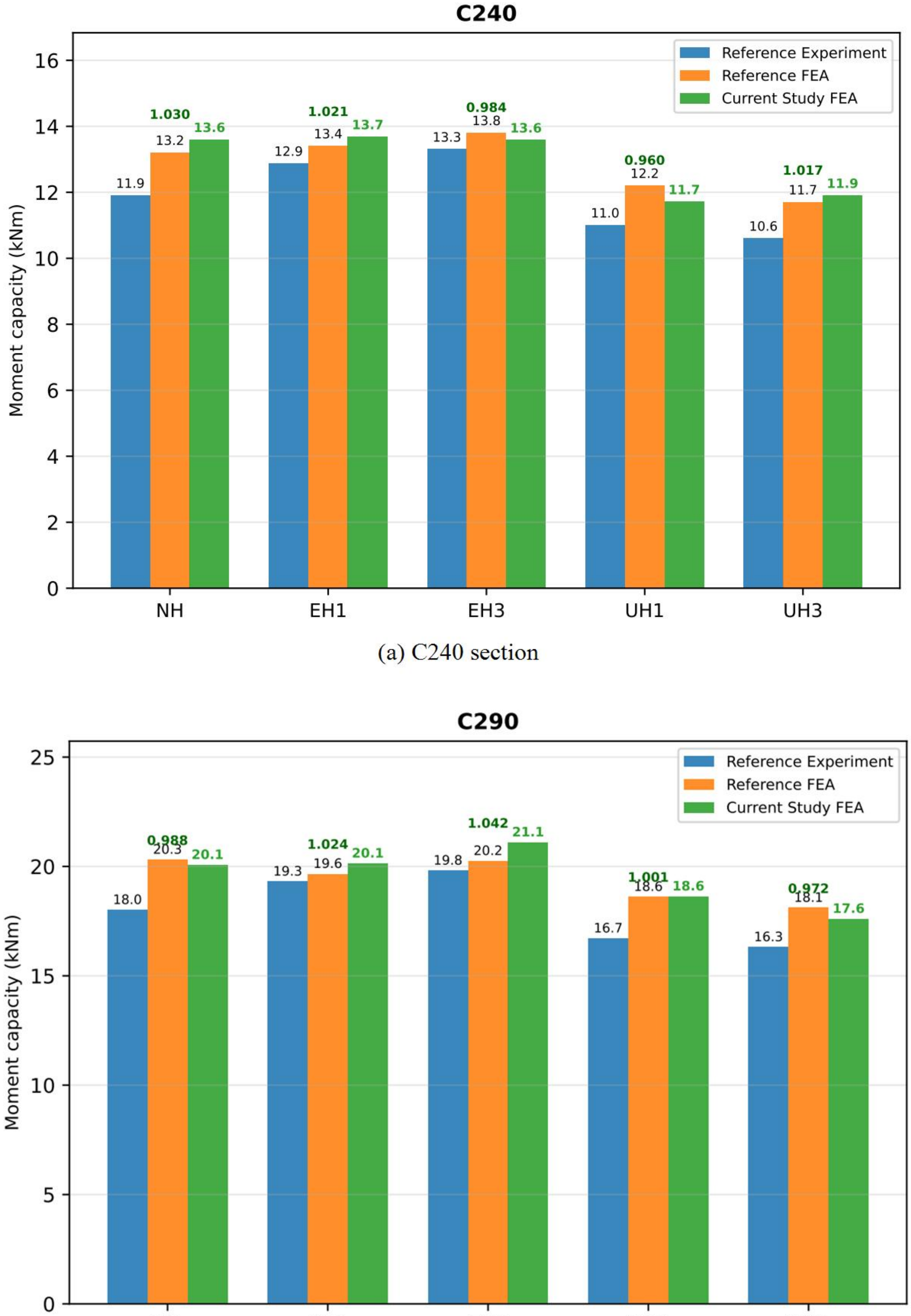

(a) C240 section

(b) C290 section

Figure 6 Comparison of moment capacities between the present FE results and the reference results reported by Chen et al. [22]: (a) C240 section; (b) C290 section.

Fig.6 compares the moment capacities from the present FE models with the reference FE. For the C240 section, the reproduced FE model gives moment capacities of 13.6 kN·m, 13.7 kN·m, 13.6 kN·m, 11.7 kN·m, and 11.9 kN·m for NH, EH1, EH3, UH1, and UH3, respectively. These values are close to the reference FE results, which are 13.2 kN·m, 13.4 kN·m, 13.8 kN·m, 12.2 kN·m, and 11.7 kN·m. The largest difference appears in the UH1 model. Even so, the difference is still within a reasonable range. The other C240 models show only small differences.

For the C290 section, the reproduced FE moment capacities are 20.1 kN·m, 20.1 kN·m, 21.1 kN·m, 18.6 kN·m, and 17.6 kN·m for NH, EH1, EH3, UH1, and UH3, respectively. The corresponding reference FE values are 20.3 kN·m, 19.6 kN·m, 20.2 kN·m, 18.6 kN·m, and 18.1 kN·m. The C290 results also show good agreement with the reference data. The largest differences are found in the EH3 and UH3 models. However, the general trend is still well captured.

Overall, the reproduced FE models give a reasonable prediction of the moment capacity for both C240 and C290 sections. Therefore, the modelling approach can be used as the basis for the later parametric study.

Fig. 7 shows the ratio of the present FE moment capacity to the reference FE moment capacity. When the ratio is close to 1.0, the reproduced result is close to the reference FE result. For the C240 section, the ratios are generally near 1.0. Slightly larger differences are found in the UH models, but the overall agreement is still acceptable. For the C290 section, the same trend can be seen. Most of the ratios stay close to 1.0, which means that the reproduced models give similar moment capacities to those reported by Chen et al. [22].

From these comparisons, the reproduced FE models were considered accurate enough for the purpose of this study. The model was then extended to the parametric study. In the later models, elongated web holes with different radii, aspect ratios, hole numbers, and clear spacings were considered. Edge-stiffened holes were also included. In addition, selected models were used to examine the effect of lip angle.

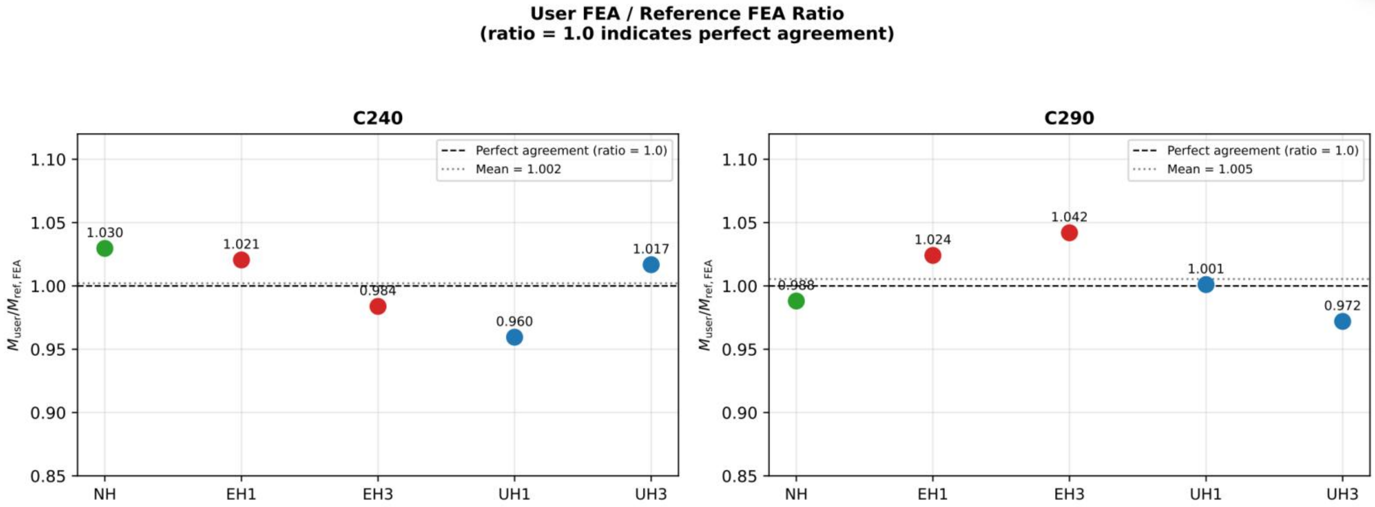

Figure 7 Validation ratios between the present FE results and the reference FE results: (a) C240 section; (b) C290 section.

3. Parametric study

3.1. General

After the FE modelling approach had been checked against the reference results in Section 2.7, it was used for the main parametric study. The study focused on cold-formed steel (CFS) C-channel beams with elongated web holes. The main question was whether a larger web opening could be provided without causing too much loss in flexural strength. Therefore, the parametric study was arranged to compare no-hole beams, beams with unstiffened elongated web holes, and beams with edge-stiffened elongated web holes.

Table 3.1

Model matrix used in the finite element study.

Model group	**Section**	**Hole shape**	**Hole type**	**Hole radius R (mm)**	**Aspect ratio ab**	**Number of holes**	**Clear spacing s (mm)**	**Lip angle**	**Number of models**
Reproduced validation models	C240, C290	Circular	NH, UH, EH	70	-	0, 1, 2, 3, 5	50, 100, or -	90°	14
UH1	C240, C290	Elongated	Unstiffened hole	70, 75, 80	1.25, 1.50, 1.75, 2.00	1	-	90°	24
EH1	C240, C290	Elongated	Edge-stiffened hole	70, 75, 80	1.25, 1.50, 1.75, 2.00	1	-	90°	24
UH2	C240, C290	Elongated	Unstiffened hole	70, 75, 80	1.25, 1.50, 1.75, 2.00	2	50, 100	90°	48

Model group	**Section**	**Hole shape**	**Hole type**	**Hole radius R (mm)**	**Aspect ratio ab**	**Number of holes**	**Clear spacing s (mm)**	**Lip angle**	**Number of models**
EH2	C240, C290	Elongated	Edge-stiffened hole	70, 75, 80	1.25, 1.50, 1.75, 2.00	2	50, 100	90°	48
UH3	C240, C290	Elongated	Unstiffened hole	70, 75, 80	1.25, 1.50, 1.75, 2.00	3	50, 100	90°	48
EH3	C240, C290	Elongated	Edge-stiffened hole	70, 75, 80	1.25, 1.50, 1.75, 2.00	3	50, 100	90°	48
Lip-angle UH1	C240, C290	Elongated	Unstiffened hole	80	1.50	1	-	20°, 45°, 60°, 75°	8
Lip-angle EH1	C240, C290	Elongated	Edge-stiffened hole	80	1.50	1	-	20°, 45°, 60°, 75°	8
Mesh convergence study									12
Total									**282**

In total, 282 finite element models were analysed in this study. The model matrix is summarised in Table 3.1. The 24 reproduced circular-hole models were used for validation and comparison with the reference study. The remaining 258 models were used for the elongated web-hole parametric study. These models included the main hole-geometry cases and the additional lip-angle cases. In this way, the table shows how the full model set was formed, rather than only giving the final number of models.

Two section depths were considered, namely C240 and C290. These were the same section groups used in the reference study. For each section, a no-hole model was analysed first. This model was used as the baseline model. The ultimate moment capacities of the C240 and C290 no-hole models were 13.591 kN·m and 20.058 kN·m, respectively. These two values were then taken as the reference moment capacities, M_0. They were later used to calculate the strength retention ratio of the corresponding web-hole models.

Before the model labels and result comparisons are introduced, the main geometric definitions need to be explained. This is because several parameters were changed in the parametric study. These include the hole radius, elongated-hole aspect ratio, clear spacing between adjacent holes, number of holes, stiffening condition, and lip angle.

Fig. 8 shows the basic geometry of the elongated web hole. In this study, the hole radius is denoted as R, and the elongated-hole aspect ratio is denoted as ab. The value of ab is defined using the overall hole length and the hole height. When R is kept unchanged, a larger ab value gives a longer elongated opening. As a result, the web opening area also becomes larger.

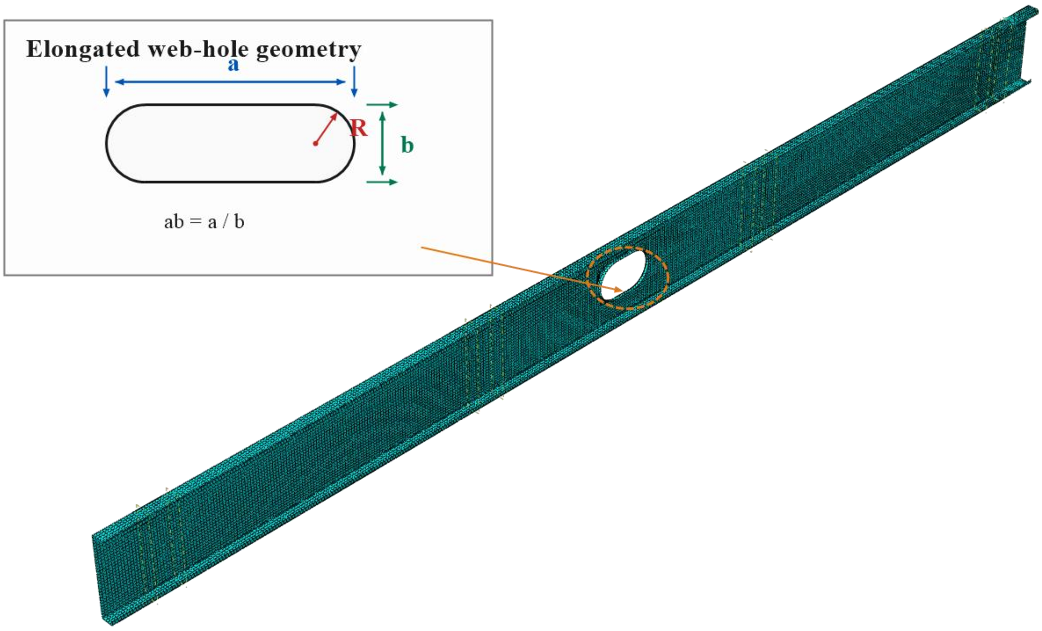

Figure 8 Definition of hole radius R and aspect ratio ab for the elongated web-hole models.

For the models with more than one web hole, the clear spacing between adjacent holes was also considered. As shown in Fig. 9, the spacing s is defined as the clear distance between two neighbouring elongated holes. Two values of clear spacing were used in this study. These were 50 mm and 100 mm. This allowed the effect of hole interaction to be examined in the two-hole and three-hole models.

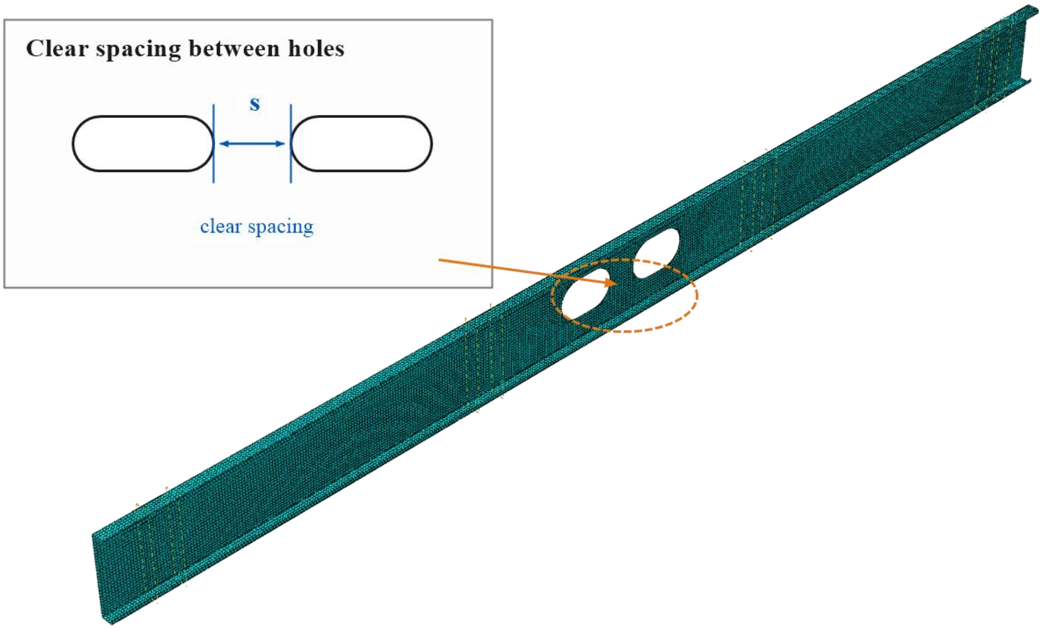

Figure 9 Definition of clear spacing s for two-hole elongated web-hole models.

Several geometric parameters were changed in the parametric study. The first parameter was the number of web holes. Models with one, two, and three holes were analysed, while the no-hole beam was used as the baseline case. The hole radius was also varied. Three radii were considered in this study: 70 mm, 75 mm, and 80 mm. For each radius, four elongated-hole aspect ratios were used, namely 1.25, 1.50, 1.75, and 2.00.

The straight length of the elongated hole depended on the selected hole radius. For the 70 mm radius holes, the straight lengths were 35 mm, 70 mm, 105 mm, and 140 mm. When the radius increased to 75 mm, the straight lengths became 37.5 mm, 75 mm, 112.5 mm, and 150 mm. For the 80 mm radius holes, the straight lengths were 40 mm, 80 mm, 120 mm, and 160 mm. Therefore, the study did not only change the radius of the hole. It also changed the length of the elongated part of the opening.

Both unstiffened hole models (UH) and edge-stiffened hole models (EH) were included. Fig. 10 shows the difference between these two opening types. In the UH models, the elongated opening was cut directly through the web. In the EH models, a stiffened edge was added around the opening. The edge stiffener length was kept as 13 mm for all EH models. The fillet radius around the stiffened opening was also kept constant at 4 mm. Keeping these two values unchanged made it easier to compare the influence of the other parameters.

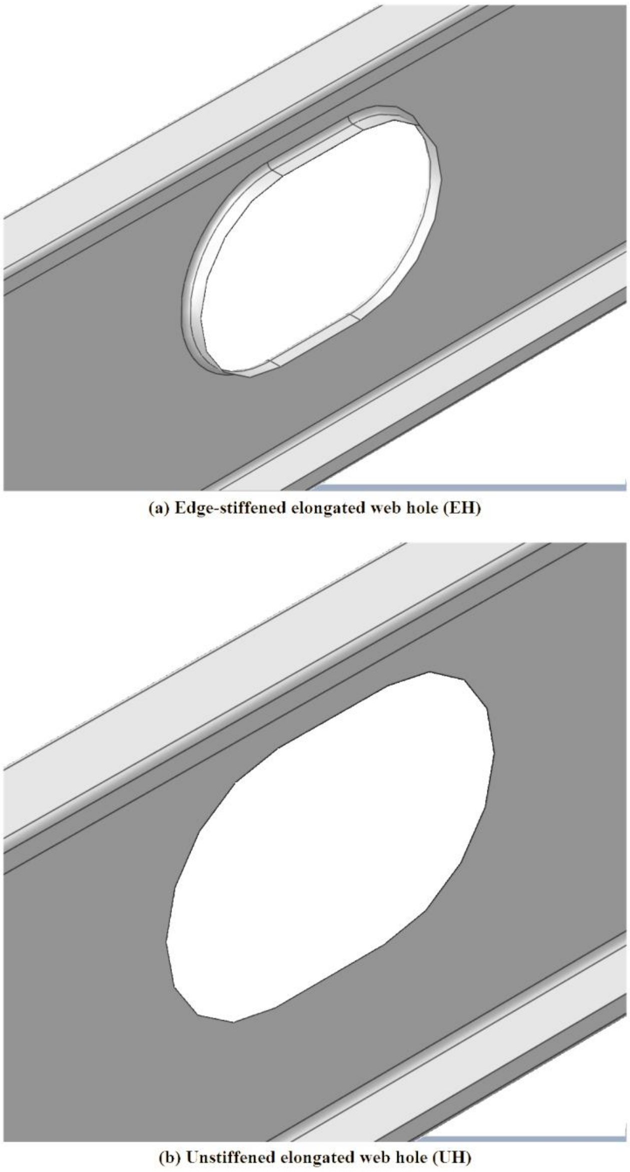

Figure 10 Local comparison between edge-stiffened and unstiffened elongated web holes.

The hole-number configurations are shown in Fig. 11. The models with one, two, and three edge-stiffened holes were labelled as EH1, EH2, and EH3, respectively. The corresponding unstiffened models were labelled as UH1, UH2, and UH3. By comparing these models, the influence of increasing the number of web openings could be studied. This comparison is important because increasing the number of holes can provide more service openings, but it may also reduce the bending strength of the member.

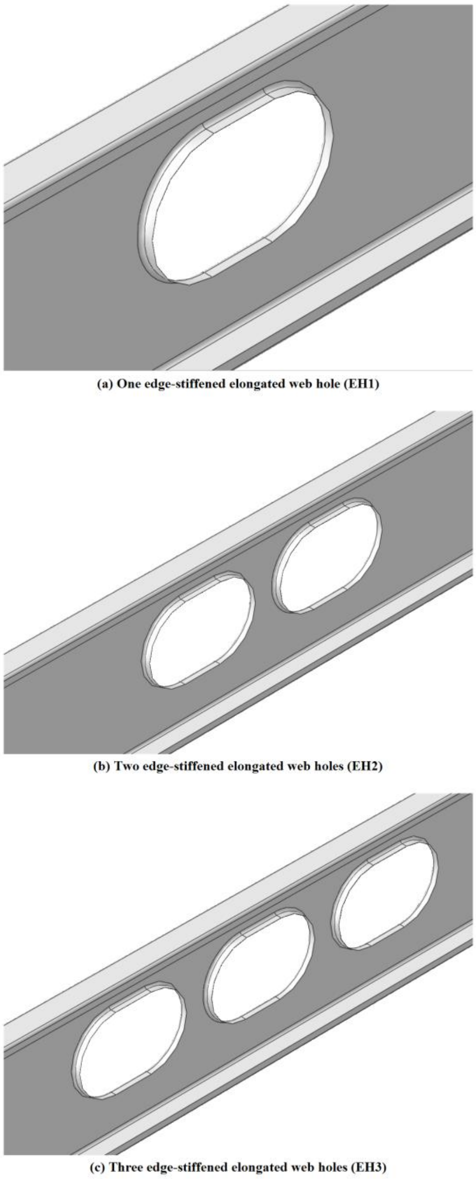

Figure 11 Edge-stiffened elongated web-hole configurations with different numbers of holes.

In addition to the web-hole parameters, selected UH1 and EH1 models were used to study the effect of lip angle. The definition of lip angle is shown in Fig. 12. The original lip angle was 90°. Four modified lip angles were considered, namely 20°, 45°, 60°, and 75°. In these models, only the lip angle was changed. The lip length was kept the same. Therefore, the influence of the C-section lip orientation could be examined separately from the web-hole parameters.

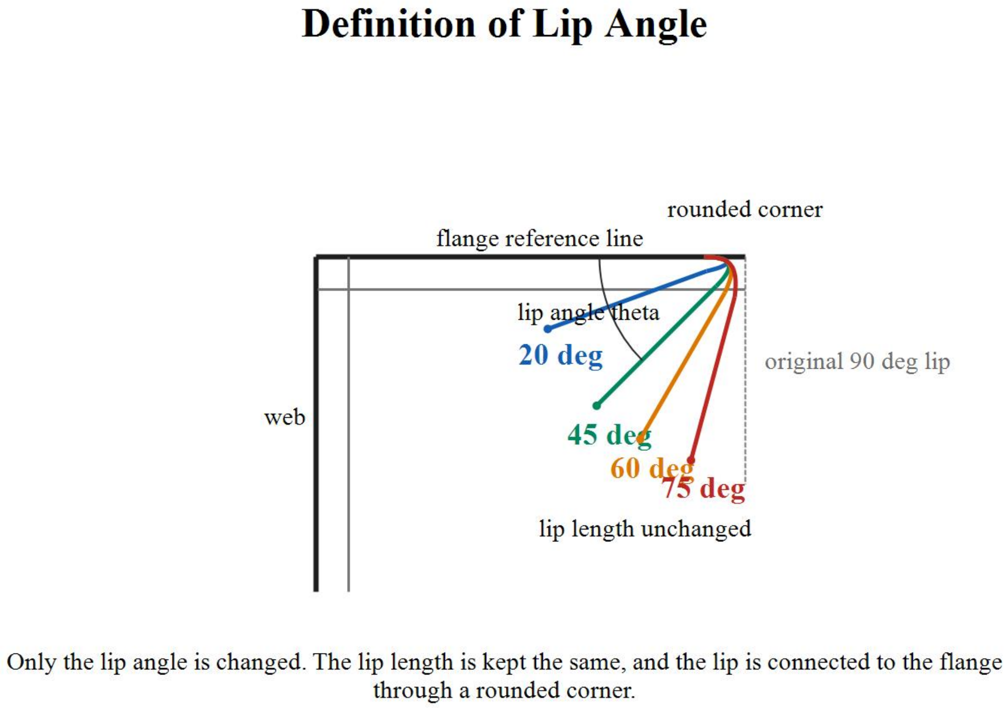

Figure 12 Definition of lip angle with rounded web-flange and flange-lip corners.

Several response quantities were extracted from the parametric models. The ultimate moment capacity Mu was obtained from the peak of the moment-displacement curve. The displacement at the peak moment was recorded as δu. To compare models with different section depths, the strength retention ratio Mu/M_0 was calculated. This was obtained by normalising the ultimate moment of each web-hole model by the corresponding no-hole baseline moment. The opening ratio ρ was also calculated to describe the relative size of the web opening area. For the edge-stiffened models, the stiffening efficiency η was used to quantify the increase in moment capacity compared with the corresponding unstiffened model.

Through these comparisons, the parametric study was used to identify which elongated web-hole configurations could provide a larger service opening area without causing excessive strength loss. Particular attention was given to the comparison between UH and EH models. The influence of increasing the hole radius from 70 mm to 80 mm was also examined. In addition, the effects of elongated-hole aspect ratio, clear spacing, hole number, and lip angle were compared. In other words, this study was not only aimed at finding the model with the highest moment capacity. A more practical question was whether a larger web opening could be provided while still maintaining an acceptable level of flexural strength. For this reason, the results were discussed in terms of both opening ratio and strength retention ratio, rather than moment capacity alone.

3.2. Model Labelling

The finite element models used in the parametric study were labelled to identify the main geometric and modelling parameters. The label of each model includes the section depth, hole type, hole radius, elongated-hole aspect ratio, clear spacing between holes, and section group. In this study, the two section groups were C240 and C290. The hole types included no-hole models (NH), unstiffened elongated web-hole models (UH), and edge-stiffened elongated web-hole models (EH).

For the web-hole models, the number following UH or EH indicates the number of holes. For example, UH1 means a beam with one unstiffened elongated web hole. Similarly, EH3 means a beam with three edge-stiffened elongated web holes. This labelling method is consistent with the hole-number configurations shown in Fig. 11. It also makes the comparison between different hole numbers clearer.

The notation HS75 or HS80 was used to identify the hole radius. HS75 refers to a hole radius of 75 mm, and HS80 refers to a hole radius of 80 mm. If no HS notation is included in the model name, the hole radius is taken as 70 mm. This convention was used throughout the result analysis.

The notation ab was used to describe the elongated-hole aspect ratio, as defined in Fig. 8. In this study, four aspect ratios were considered. The notation ab125 represents an aspect ratio of 1.25, ab15 represents an aspect ratio of 1.50, ab175 represents an aspect ratio of 1.75, and ab20 represents an aspect ratio of 2.00. The corresponding straight length of the elongated hole depends on the hole radius. For example, for HS80 models, ab125, ab15, ab175, and ab20 correspond to straight lengths of 40 mm, 80 mm, 120 mm, and 160 mm, respectively.

For two-hole and three-hole models, the spacing notation was also included in the model label. The notation s50 or space50 indicates a clear spacing of 50 mm between adjacent holes. Similarly, s100 or space100 indicates a clear spacing of 100 mm. The meaning of this spacing is shown in Fig. 9. For single-hole models, the clear spacing is not physically relevant. Therefore, if a single-hole model contains s50 or s100 in the name, it is treated as the same physical model.

For example, the model label “UH2-HS80-ab125-s50-240” can be interpreted as follows:

• The notation “UH2” refers to a beam with two unstiffened elongated web holes;

• The notation “HS80” refers to a hole radius of 80 mm;

• The notation “ab125” refers to an elongated-hole aspect ratio of 1.25. For an 80 mm hole radius, this corresponds to a straight length of 40 mm;

• The notation “s50” refers to a clear spacing of 50 mm between adjacent holes;

• The number “240” refers to the C240 section group.

Similarly, the model label “EH3-HS80-ab175-s100-290” can be interpreted as follows:

• The notation “EH3” refers to a beam with three edge-stiffened elongated web holes;

• The notation “HS80” refers to a hole radius of 80 mm;

• The notation “ab175” refers to an elongated-hole aspect ratio of 1.75. For an 80 mm hole radius, this corresponds to a straight length of 120 mm;

• The notation “s100” refers to a clear spacing of 100 mm between adjacent holes;

• The number “290” refers to the C290 section group.

The edge-stiffened hole models used the prefix EH. As shown in Fig. 10, the EH models include a stiffened edge around the elongated web opening. For all EH models, the edge stiffener length was kept as 13 mm and the fillet radius around the stiffened opening was kept as 4 mm. These two values were not repeated in every model name because they were kept constant throughout the EH models.

In addition, selected models were used to study the effect of lip angle. These models were labelled using the notation lip20, lip45, lip60, and lip75. The definition of the lip angle is shown in Fig. 12. For example, the label “240-EH1-HS80-ab15-lip45” refers to a C240 beam with one edge-stiffened elongated web hole, a hole radius of 80 mm, an aspect ratio of 1.50, and a lip angle of 45°. In these models, the lip length was unchanged, and only the lip angle was modified.

The no-hole baseline models were labelled as NH. In the result analysis, the C240 and C290 no-hole models were treated separately. Their ultimate moment capacities were used as the reference moment capacities M_0 for calculating the strength retention ratio of the corresponding web-hole models.

4. Results and discussion

4.1. General

This chapter presents the results obtained from the parametric finite element study. After the FE modelling method was checked in Chapter 2, it was used to analyse a wider group of CFS channel beams with elongated web holes. In total, 282 FE models were included. These models covered no-hole beams, beams with unstiffened elongated web holes, and beams with edge-stiffened elongated web holes. Both C240 and C290 sections were considered.

The main purpose of this chapter is to examine how the web-hole parameters influence the flexural behaviour of the beams. The parameters include hole radius, elongated-hole aspect ratio, clear spacing between adjacent holes, number of holes, edge stiffening, and lip angle. These parameters were selected because they directly affect the available service opening area and the moment capacity of the beam.

Several response quantities are used in the following discussion. The ultimate moment capacity is denoted as Mu, and it is taken as the peak value of the moment-displacement curve. The displacement corresponding to this peak moment is denoted as du. The no-hole models are used as the baseline cases. The ultimate moment capacity of the no-hole model is denoted as M_0. In this study, the C240 baseline moment capacity is 13.591 kN.m, while the C290 baseline moment capacity is 20.058 kN.m. These two values are then used to calculate the strength retention ratio, Mu/M_0, for the corresponding web-hole models.

In addition to moment capacity, the opening ratio rho is also used. This value describes the relative size of the web opening area. Therefore, it is useful for comparing models with different hole sizes and different numbers of holes. For the edge-stiffened models, the stiffening efficiency eta is also used to show how much strength is recovered by adding the stiffened edge around the opening. Similar response quantities were also used in previous studies on CFS members with web holes, where moment capacity, strength reduction, and opening geometry were important indicators for evaluating the structural effect of web openings [22].

Since the full parametric study contains a large number of models, it is not practical to list all 282 results in the main text. Therefore, selected representative models are first presented in Table 4.1. The table follows the same general logic as the specimen table reported by Chen et al. [22], but the moment capacities in this study are obtained from FEA rather than physical tests. The table includes the main section dimensions, hole size, clear spacing, predicted moment capacity, and the percentage of strength change due to holes.

For the elongated web-hole models, the hole size A in Table 4.1 represents the hole height, which is equal to 2R. The elongated-hole length is controlled separately by the aspect ratio ab, as defined in Chapter 3. Therefore, Table 4.1 should be read together with the geometric definitions given earlier. This is especially important because two models with the same hole height can still have different opening areas if their ab values are different.

Table 4.1

Selected specimen dimensions and finite element moment capacities.

Specimen	Web (mm)	Flange (mm)	Lip(mm)	Length (mm)	Thickness (mm)	Hole size (mm)	Hole spacing (mm)	Moment capacity MFEA (kN*m)	Strength change due to holes (%)
NH-240	240	45	15	4000	1.83	-	-	13.591	-
UH1-HS80-ab15	240	45	15	4000	1.83	160	-	11.328	-16.65
EH1-HS80-ab15-240	240	45	15	4000	1.83	160	-	12.319	-9.36
UH2-HS80-ab125-s50-240	240	45	15	4000	1.83	160	50	11.486	-15.49
EH2-HS80-ab125-s50-240	240	45	15	4000	1.83	160	50	12.658	-6.87
UH2-HS80-ab125-s100-240	240	45	15	4000	1.83	160	100	11.572	-14.86
EH2-HS80-ab125-s100-240	240	45	15	4000	1.83	160	100	12.563	-7.56
UH3-HS80-ab125-s50-240	240	45	15	4000	1.83	160	50	11.51	-15.31
EH3-HS80-ab125-s50-240	240	45	15	4000	1.83	160	50	12.473	-8.23
NH-290	290	45	15	4000	2.11	-	-	20.058	-

UH1-HS80-ab15-s50-290	290	45	15	4000	2.11	160	-	16.856	-15.96
EH1-HS80-ab15-s100-290	290	45	15	4000	2.11	160	-	20.223	0.82
UH2-HS80-ab125-s50-290	290	45	15	4000	2.11	160	50	17.553	-12.49
EH2-HS80-ab125-s50-290	290	45	15	4000	2.11	160	50	20.783	3.61
UH2-HS80-ab125-s100-290	290	45	15	4000	2.11	160	100	16.818	-16.15
EH2-HS80-ab125-s100-290	290	45	15	4000	2.11	160	100	20.513	2.27
UH3-HS80-ab125-s50-290	290	45	15	4000	2.11	160	50	16.991	-15.29
EH3-HS80-ab125-s50-290	290	45	15	4000	2.11	160	50	20.299	1.2

The results in Table 4.1 give an initial view of the main trends. For example, the C240 no-hole model gives a baseline moment capacity of 13.591 kN.m, while the C290 no-hole model gives 20.058 kN.m. When unstiffened holes are introduced, the moment capacity generally decreases. However, when edge stiffening is added around the openings, part of this strength loss is recovered. In some C290 edge-stiffened cases, the predicted moment capacity is even close to or slightly higher than the no-hole baseline value.

The detailed discussion is then developed step by step. First, the moment-displacement behaviour of selected web-hole models is compared. After that, the effects of edge stiffening, hole radius, elongated-hole aspect ratio, clear spacing, number of holes, and lip angle are discussed separately. The discussion does not only focus on the model with the largest moment capacity. Instead, more attention is given to the balance between opening area and strength retention. This is important for practical applications, because elongated web holes are mainly used to provide larger service openings while keeping the reduction in flexural capacity within an acceptable range.

The modelling method used in this study was based on the work of Chen et al. [22]. However, the aim of the present parametric study is not exactly the same. In the reference study, the web openings were circular. The main variables were hole diameter, number of holes, stiffener length, and fillet radius. In this study, the web openings are elongated. Because of this change, the hole geometry cannot be described only by the hole diameter. The hole radius, straight length, aspect ratio, and clear spacing also need to be considered.

For this reason, Table 4.2 is included to show the difference between the reference parametric study and the present study. This table also helps to explain why some new parameters, such as ab and s, are used in the following discussion.

Table 4.2

Comparison between the reference parametric study and the present parametric study.

Item	Reference study by Chen et al. [22]	Present study
Section type	CFS channel beams	CFS C-channel beams
Section depth	240 mm and 290 mm	C240 and C290
Beam length	4000 mm for Table 6 models	4000 mm
Hole shape	Circular web holes	Elongated web holes
Hole type	Edge-stiffened web holes	Unstiffened elongated holes and edge-stiffened elongated holes
Number of holes	1, 3, and 5 holes	1, 2, and 3 holes
Hole size parameter	Hole diameter A	Hole radius R and elongated-hole aspect ratio ab
Hole size range	A/d = 0.1, 0.3, and 0.5	R = 70, 75, and 80 mm; ab = 1.25, 1.50, 1.75, and 2.00
Hole spacing	Mainly used for multi-hole specimens	Clear spacing s = 50 mm and 100 mm
Edge stiffener length	Varied using Q = q/d = 0.04, 0.06, and 0.08	Fixed at 13 mm
Fillet radius	Varied using rq/t = 1, 2, and 3	Fixed at 4 mm
Lip angle	Not considered as a main parameter	20°, 45°, 60°, 75°, and 90°
Main output	Moment capacity predicted from FEA, MFEA	Ultimate moment capacity Mu, displacement at peak moment δu, strength retention ratio M_u/M_0, opening ratio ρ, and stiffening efficiency η
Main purpose	To study the effects of hole diameter, stiffener length, fillet radius, and hole number on moment capacity	To increase elongated web-hole area while keeping the reduction in flexural strength within an acceptable range

It can be seen from Table 4.2 that the present study is an extension of the reference work rather than a direct repetition of it. The edge stiffener length and the fillet radius were kept constant in this study. Their values were 13 mm and 4 mm, respectively. By doing this, the influence of the elongated-hole geometry can be seen more clearly. In other words, the changes in the results are mainly related to the hole radius, the length of the elongated opening, the clear spacing between holes, and the lip angle.

Another difference is the number of holes. Chen et al. [22] considered one, three, and five circular holes. In the present study, one, two, and three elongated holes were selected. This was not only for simplicity. It was also related to the geometry of the test region. Since an elongated hole is much longer than a circular hole, five elongated openings would occupy too much length along the beam. In that case, some holes could move outside the constant moment region. Therefore, five-hole elongated models were not included in this study.

Based on this comparison, the following sections discuss the main parameters one by one. The discussion first considers the moment-displacement behaviour. It then examines the effects of edge stiffening, hole radius, aspect ratio, clear spacing, number of holes, and lip angle. The purpose is to identify which combinations can provide a larger opening area while still keeping an acceptable level of moment capacity.

4.2. Moment-displacement behaviour

The moment-displacement responses of the no-hole reference models were discussed previously in Section 2.7 and Fig. 3 and are therefore not repeated here. This section focuses on representative models containing unstiffened holes (UH) and edge-stiffened holes (EH). The comparison examines the initial stiffness, peak moment, displacement at peak moment, and post-peak response.

Moment-displacement curves provide more information than the maximum moment alone. They indicate whether the introduction of web holes or edge stiffeners changes the initial elastic response and show how rapidly the resistance decreases after the peak. This is important because models with similar peak moments may exhibit different post-peak responses. A similar curve-based approach was adopted by Chen et al. [22] when validating their FE models against experimental results. Chandramohan et al. [34] also investigated the flexural behaviour and moment capacity of CFS channel beams with elongated edge-stiffened and unstiffened web holes through an extensive numerical study.

Figure. 13 compares three representative pairs of UH and EH models. The selected cases include two C290 three-hole models and one C240 single-hole model. They cover different section sizes, numbers of openings, opening aspect ratios, and clear spacings.

In all three comparisons, the UH and EH curves are almost identical during the initial linear stage. This indicates that edge stiffening has a limited influence on the overall elastic stiffness of the beam. The main difference develops as the models approach their peak moments. In each case, the EH model reaches a higher peak moment and reaches that peak at a larger displacement than the corresponding UH model. This behaviour indicates that edge stiffening mainly affects the nonlinear response close to failure rather than the initial elastic response.

Figure. 13(a) presents the C290 three-hole model with R = 70 mm, a/b = 1.25, and s = 100 mm. The UH response begins to lose stiffness and reaches its peak earlier than the EH response. The EH model reaches a moment slightly higher than the no-hole reference value of M0 = 20.058 kN m. This result indicates that edge stiffening can recover a substantial proportion of the capacity lost because of the three elongated openings.

After reaching its peak, the EH model experiences an initial reduction in moment followed by a relatively stable residual response. Its moment remains consistently higher than that of the UH model, whose resistance decreases more continuously with increasing displacement. Therefore, edge stiffening improves both the peak moment and the absolute residual resistance in this case.

Figure. 13(b) shows the C290 three-hole model with R = 70 mm, a/b = 2.0, and s = 50 mm. This arrangement contains longer and more closely spaced openings and therefore represents a more demanding configuration. The UH model reaches a noticeably lower peak moment, whereas the EH model retains a peak moment close to M0. The comparison shows that edge stiffening remains effective even when the opening length is increased and the clear spacing is reduced.

However, the EH model in Fig. 13(b) exhibits a pronounced reduction in moment immediately after its peak. As the displacement approaches 30 mm, the UH and EH curves become relatively close. This indicates that edge stiffening mainly improves the peak capacity and delays the peak response in this model, while providing a smaller improvement in the long-displacement residual resistance.

Figure. 13(c) presents the C240 single-hole model with R = 70 mm and a/b = 2.0. The EH model again reaches a higher peak moment and a larger displacement at peak than the corresponding UH model. Therefore, the beneficial effect of edge stiffening is not limited to the C290 section or to models containing multiple openings.

The EH model in Fig. 13(c) remains above the UH model after the peak, indicating a higher absolute residual moment. However, the reduction relative to its own peak is still considerable. Consequently, a higher residual moment should not automatically be interpreted as improved ductility because the EH model also begins its post-peak response from a higher peak capacity.

Overall, Fig. 13 shows that edge stiffening has little influence on the initial elastic stiffness but produces a clear improvement in the nonlinear response near the peak moment. The EH models consistently achieve higher peak moments and reach their peaks at larger displacements. However, the effect on post-peak behaviour depends on the opening arrangement and section geometry. Some EH models retain a clear residual-strength advantage, whereas others lose a substantial proportion of their peak resistance and gradually approach the corresponding UH response. The benefit of edge stiffening is therefore more consistent for peak capacity than for post-peak stability. The strength improvement and associated stress redistribution are examined further in Section 4.3.

4.3. Effect of unstiffened and edge-stiffened holes

Figure. 13 compares the moment-displacement responses of representative models with unstiffened holes (UH) and edge-stiffened holes (EH). The effects of edge stiffening are further quantified using the strength retention ratio, M_u/M_0, and the stiffening efficiency. The results generally show that the EH models achieve higher peak moments than the corresponding UH models. This trend is consistent with Chandramohan et al. [34], who reported that beams with elongated edge-stiffened web holes achieved an average moment capacity approximately 9 percent higher than beams with corresponding unstiffened openings.

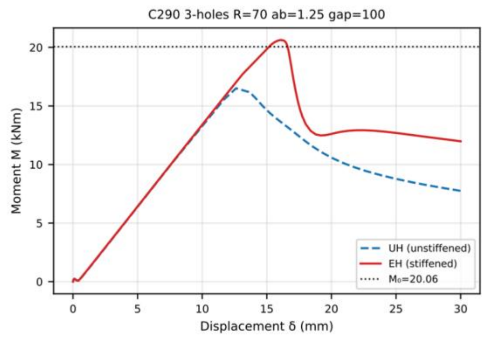

(a) C290 3-hole model, R = 70 mm, ab = 1.25, s = 100 mm

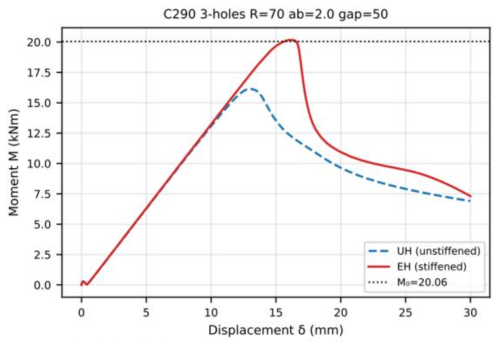

(b) C290 3-hole model, R = 70 mm, ab = 2.0, s = 50 mm

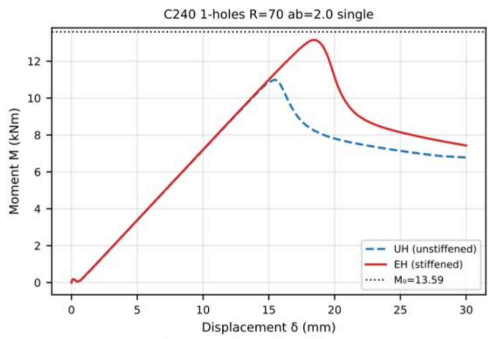

(c) C240 1-hole model, R = 70 mm, ab = 2.0

Figure 13 Comparison of moment-displacement curves between unstiffened and edge-stiffened elongated web-hole models.

The difference between the UH and EH models may be attributed to the local stiffness provided by the edge stiffener. An unstiffened opening interruptss the load-transfer path through the web and forms a relatively flexible hole boundary. This promotes deformation around the opening and may cause the capacity-limiting response to develop before the remaining section reaches its full flexural resistance. In comparison, the edge stiffener restrains deformation along the hole boundary and redistributes stresses into the surrounding web and flanges.

For the C290 three-hole model with R=70 mm, a/b=1.25, and s=100 mm, the UH model gives a strength retention ratio of approximately 0.823. The corresponding EH model reaches approximately 1.028, giving a stiffening efficiency of 24.95%. This increase indicates that the stiffened boundary substantially reduces the local weakening caused by the openings. However, this result should not be interpreted as evidence that the holes inherently improve beam strength. Instead, within the analysed FE model range, the edge stiffener locally increases stiffness and modifies the structural response sufficiently for the predicted capacity to become slightly higher than that of the no-hole reference model.

A similar response is obtained for the C290 three-hole model with R=70 mm, a/b=2.0, and s=50 mm. The UH model has a strength retention ratio of approximately 0.805, whereas the corresponding EH model reaches approximately 1.006. The resulting stiffening efficiency is 24.95%. The longer openings and smaller spacing increase the interaction between the locally weakened regions. Nevertheless, edge stiffening remains effective because it restrains deformation along the elongated hole boundaries and improves load transfer through the web between adjacent openings.

For the C240 single-hole model with R=70 mm and a/b=2.0, the strength retention ratio increases from approximately 0.809 for the UH model to 0.968 for the EH model, corresponding to a stiffening efficiency of 19.61%. Although the EH model does not fully recover the capacity of the no-hole model, the improvement confirms that the stiffened hole boundary reduces the adverse influence of the opening. The smaller recovery compared with the selected C290 cases suggests that stiffening effectiveness also depends on the section geometry and its interaction with the opening.

Figure. 14 compares the von Mises stress distributions of the representative UH and EH models at approximately the same displacement of 19.6 mm. A common contour range of 0–430 MPa was used. In the UH model, relatively high stresses are concentrated around the unstiffened opening and the adjacent web. In comparison, the stiffened hole boundary modifies the stress distribution and transfers stresses into a wider region of the surrounding web and flanges. This response is consistent with the increased local stiffness provided by the edge stiffener.

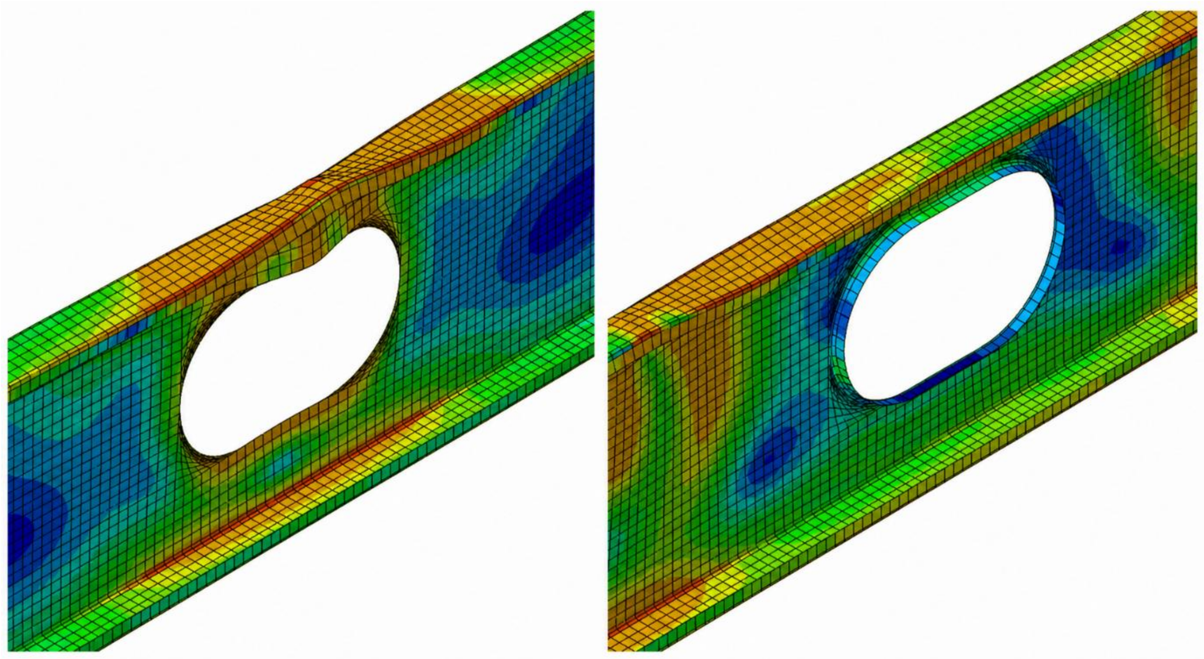

Figure 14 Von Mises stress distributions of the representative models at a displacement of approximately 19.6 mm: (a) UH model; and (b) EH model.

The curves in Fig. 13 also show that the EH models generally reach their peak moments at larger displacements than the corresponding UH models. This behaviour is consistent with a delayed capacity-limiting response around the opening. However, the EH curves exhibit a relatively rapid reduction in moment after the peak. Therefore, the benefit of edge stiffening is more evident in the peak moment capacity than in post-peak stability. A higher peak capacity should not automatically be interpreted as improved ductility.

Overall, edge stiffening can recover a substantial proportion of the moment capacity lost in UH models. Its effectiveness depends on the section size, opening geometry, number of openings, and spacing. The results indicate that edge stiffening increases local stiffness, restrains deformation around the opening, and modifies stress distribution within the analysed FE models. Nevertheless, it does not guarantee that every EH model will reach or exceed the capacity of the corresponding no-hole beam.

4.4. Effect of hole radius

Figure. 15 compares representative C290 EH models with hole radii of R = 70 mm and R = 80 mm. Within each comparison, the number of openings, opening aspect ratio, and clear spacing are kept constant. The principal variable is therefore the hole radius. Hole size was also considered an important parameter by Chen et al. [22], although their study mainly examined circular web holes rather than the elongated openings considered here.

Increasing the radius from 70 mm to 80 mm increases the opening height from 140 mm to 160 mm. For a constant opening aspect ratio, it also increases the overall opening length and opening area. Consequently, less web material remains available to transfer stresses around the opening. The radius effect is therefore related not only to the local hole-edge geometry but also to the increase in opening ratio.

During the initial loading stage, the R = 70 mm and R = 80 mm curves are generally close. This indicates that the increase in radius has a limited effect on the overall elastic stiffness of the selected EH models. The initial response is mainly controlled by the stiffness of the complete beam section, while the influence of the opening becomes more significant as local deformation develops around the hole.

The peak moments of the selected R = 80 mm models also remain relatively close to those of the corresponding R = 70 mm models and, in several cases, remain close to the no-hole reference capacity M0. This suggests that the edge stiffener can compensate for part of the local stiffness lost when the opening radius is increased. However, this should not be interpreted as evidence that increasing the radius has no adverse structural effect.

The influence of radius becomes clearer after the peak. In most of the selected comparisons, the R = 80 mm models exhibit a more rapid reduction in moment than the corresponding R = 70 mm models. This response is consistent with the smaller remaining web area and the increased susceptibility of the larger opening region to local deformation. Therefore, a model may retain a relatively high peak moment while exhibiting a less stable post-peak response.

The effect may become more important in models containing multiple openings because increasing the radius increases the total removed web area and may strengthen the interaction between adjacent opening regions. The response nevertheless depends on the opening aspect ratio, hole spacing, and number of openings. Hole radius should therefore not be treated as an independent predictor of moment capacity.

From a practical perspective, increasing the hole radius provides more space for building services, but the resulting model should be evaluated using both peak capacity and post-peak response. The results indicate that edge stiffening can limit the reduction in peak moment associated with a larger radius, but it does not necessarily prevent a more rapid post-peak loss of resistance. The practical selection of hole radius should therefore consider Mu/M0 together with the complete moment-displacement response and the corresponding opening ratio.

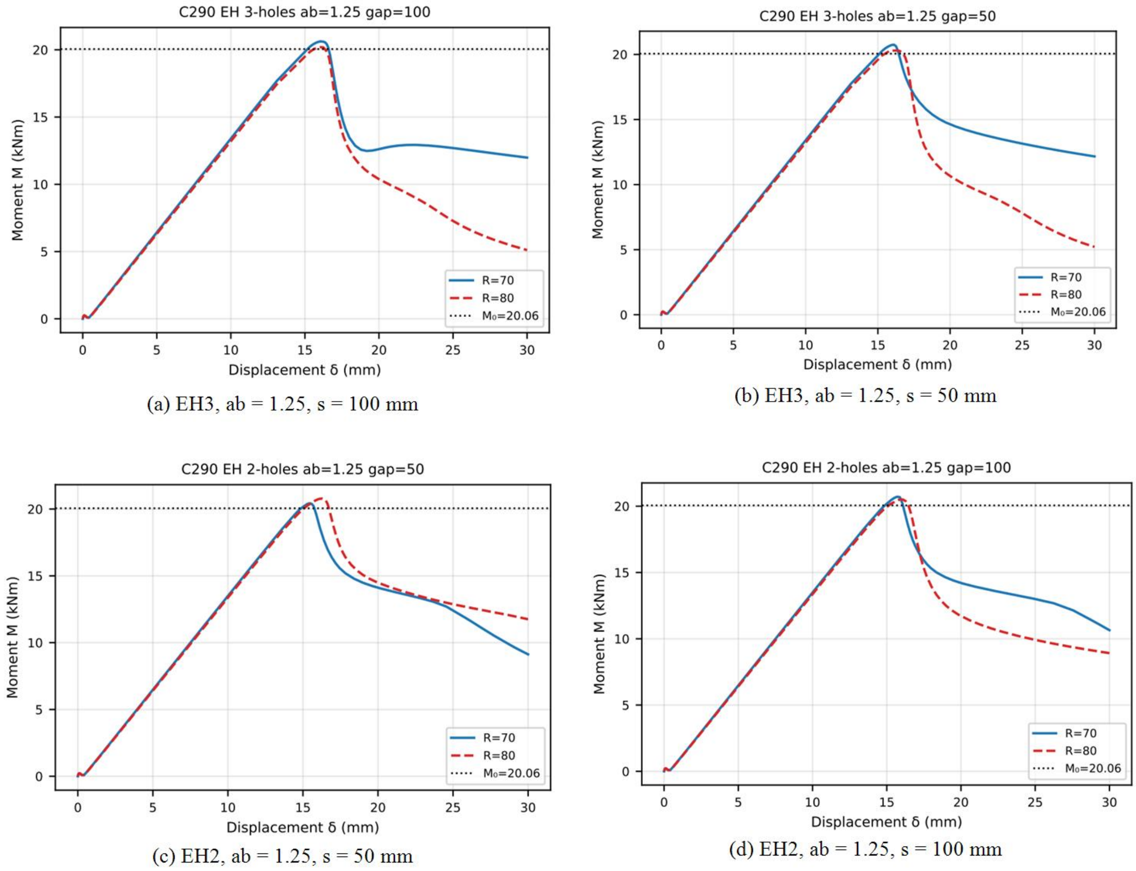

(a) EH3, ab = 1.25, s = 100 mm

(b) EH3, ab = 1.25, s = 50 mm

(c) EH2, ab = 1.25, s = 50 mm

(d) EH2, ab = 1.25, s = 100 mm

Figure 15 Effect of hole radius on the moment-displacement behaviour of C290 edge-stiffened web-hole models

4.5. Effect of elongated-hole aspect ratio

Figure. 16 compares representative C290 EH models with different elongated-hole aspect ratios. Within each comparison, the hole radius, number of openings, and clear spacing are kept constant. The principal variable is therefore the opening aspect ratio, a/b.

Increasing a/b extends the opening in the longitudinal direction while its height remains unchanged. This increases both the length and area of the opening and enlarges the region of the web affected by the opening. In multi-hole models, a larger aspect ratio also increases the total perforated length of the beam, even when the clear spacing between adjacent openings remains constant.

The curves are generally close during the initial linear stage. This indicates that changing the aspect ratio has a limited effect on the overall elastic stiffness of the selected models. At this stage, the response is mainly controlled by the stiffness of the complete beam section. The influence of opening length becomes more significant as the response approaches the peak moment.

For the smaller and intermediate aspect ratios, the EH models generally retain peak moments close to the no-hole reference capacity M0. This indicates that the edge stiffener can maintain the local rigidity of the opening boundary when the opening is moderately elongated. However, the peak moment tends to decrease when a/b reaches its largest investigated value, particularly when the larger aspect ratio is combined with a larger radius or multiple openings.

This reduction can be attributed to the greater amount of web material removed and the increased length of the opening boundary. A longer opening creates a larger flexible region in the web and increases the length over which stresses must be transferred around the hole. Although the edge stiffener restrains the hole boundary, its ability to compensate for the removed web material becomes less effective as the opening length increases.

The effect of aspect ratio is also evident in the post-peak response. In several comparisons, models with larger a/b values exhibit a more rapid reduction in moment after reaching the peak. This response is consistent with greater local deformation around the longer opening. Therefore, a model with a relatively large aspect ratio may retain a reasonable peak moment but exhibit a less stable post-peak response.

The influence of a/b is not independent of the other geometric parameters. Its effect becomes more pronounced when combined with a larger radius, a greater number of openings, or a smaller clear spacing. The aspect ratio should therefore not be assessed without considering the resulting opening ratio and the interaction between adjacent opening regions.

From a practical perspective, increasing a/b provides a longer service opening without increasing its height. However, the increase in usable opening length must be balanced against the possible reduction in peak capacity and post-peak resistance. The results indicate that edge stiffening remains effective for moderately elongated openings, but its benefit becomes less consistent at the largest investigated aspect ratios. The selection of a/b should therefore consider Mu/M0, the complete moment-displacement response, and the corresponding opening ratio.

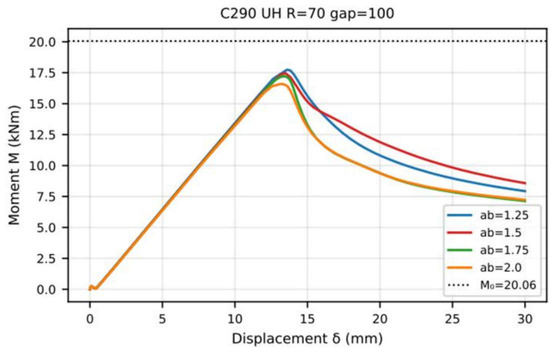

(a) UH2, R = 70 mm, s = 100 mm

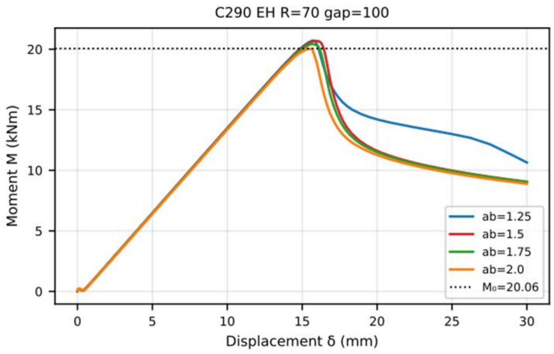

(b) EH2, R = 70 mm, s = 100 mm

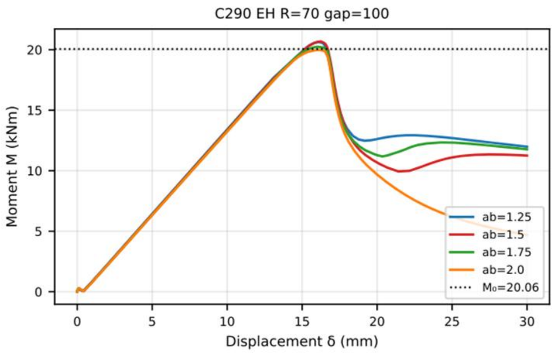

(c) EH3, R = 70 mm, s = 100 mm

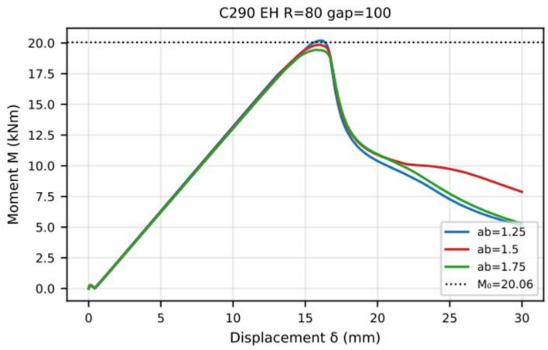

(d) EH3, R = 80 mm, s = 100 mm

Figure 16 Effect of elongated-hole aspect ratio on the moment-displacement behaviour of C290 web-hole models.

4.6. Effect of clear spacing between holes

The clear spacing between adjacent openings was investigated for the two-hole and three-hole models. Two spacing values, s = 50 mm and s = 100 mm, were considered. Within each comparison, the hole radius, opening aspect ratio, number of openings, and edge-stiffening details were kept constant.

Chen et al. [22] also considered clear spacings of 50 mm and 100 mm for circular web holes with a diameter of 140 mm. The same spacing values were adopted in the present study for elongated openings. However, the influence of spacing was evaluated together with the opening radius, aspect ratio, and number of openings because these parameters determine the interaction between adjacent opening regions.

Changing the clear spacing does not change the total area of web material removed. Instead, it changes the longitudinal distribution of the openings, the interaction between adjacent hole-edge deformation regions, and the positions of the outer openings relative to the loading points.

Consequently, spacing is expected to have a smaller influence on the initial stiffness and peak moment than parameters that directly increase the opening area.

Figure 17 compares three representative pairs of C290 EH models. The first two comparisons contain three openings, while the third contains two openings. In each pair, only the clear spacing is changed.

Figure. 17(a) presents the three-hole model with R = 70 mm and a/b = 2.0. The models with s = 50 mm and s = 100 mm exhibit similar initial stiffnesses and peak moments. However, after the peak, the model with s = 50 mm maintains a slightly higher moment than the model with s = 100 mm. This result shows that increasing the spacing does not necessarily improve the residual resistance.

One possible explanation is that, in an EH model, closely spaced stiffened boundaries and the web strip between adjacent openings may interact and provide additional local restraint. At the same time, smaller spacing can also increase the interaction between local deformation zones. The resulting response therefore depends on which of these effects becomes dominant and should not be interpreted as a general advantage of smaller spacing.

Figure. 17(b) compares the three-hole models with R = 80 mm and a/b = 1.25. The initial portions and peak moments of the two curves are again similar. Both models exhibit a relatively rapid post-peak reduction. In this comparison, the influence of the larger opening radius appears to be more significant than the change in spacing. The spacing effect is therefore secondary to the local response produced by the larger openings.

Figure. 17(c) presents the two-hole model with R = 70 mm and a/b = 1.25. In this case, the model with s = 100 mm achieves a slightly higher peak moment and maintains a higher post-peak resistance than the model with s = 50 mm. The larger spacing may reduce the interaction between the local deformation regions surrounding the two openings. This trend differs from that observed in Fig. 4.5(a), confirming that spacing interacts with the number and geometry of the openings.

Overall, the effect of clear spacing is not monotonic. Increasing s from 50 mm to 100 mm does not consistently increase either the peak moment or the post-peak resistance. The limited variation in initial stiffness and peak moment is consistent with the unchanged total opening area, while the differences after the peak are associated with local interaction between adjacent opening regions and their longitudinal positions in the beam.

Clear spacing should therefore not be used as an independent indicator of structural performance. It should be evaluated together with the number of openings, hole radius, aspect ratio, and edge-stiffening arrangement. Within the investigated range, no single spacing value can be identified as optimal for all models.

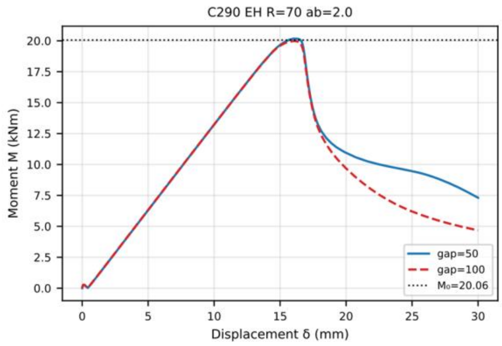

(a) EH3, R = 70 mm, ab = 2.0

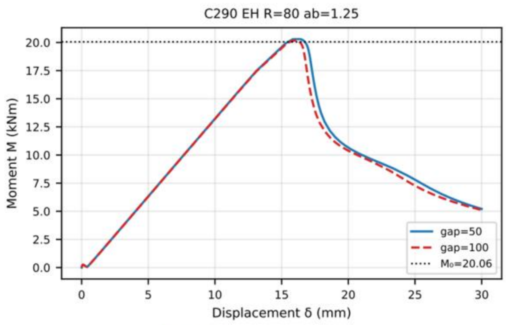

(b) EH3, R = 80 mm, ab = 1.25

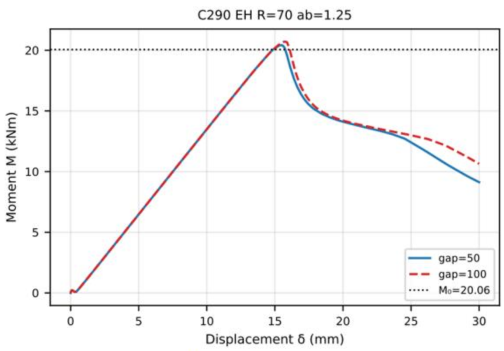

(c) EH2, R = 70 mm, ab = 1.25

Figure 17 Effect of clear spacing on the moment-displacement behaviour of C290 edge-stiffened web-hole models.

4.7. Effect of number of web holes

The number of web openings directly affects the total area of material removed from the web. Although the effects of hole radius, aspect ratio, and clear spacing were considered separately in the previous sections, practical beams may require several service openings. It is therefore necessary to evaluate how increasing the number of openings affects the opening ratio and moment capacity.

Chen et al. [22] investigated beams containing one, three, and five circular web holes. In the present study, one-hole, two-hole, and three-hole arrangements were considered. Five-hole arrangements were not included because the elongated openings occupy a greater length of the beam than circular holes of the same height. For some investigated geometries, five elongated openings would extend beyond the constant-moment region and would therefore not provide a consistent comparison.

Figure 18 compares models with R = 70 mm and a/b = 1.25. For the two-hole and three-hole models, a clear spacing of s = 100 mm was used. The opening geometry was therefore kept constant while the number of openings was varied.

As expected, the opening ratio increases almost linearly with the number of openings. For the C290 models, it increases from 1.75 percent for one opening to 5.25 percent for three openings. For the C240 models, it increases from 2.11 percent to 6.34 percent. Increasing the number of openings therefore provides a larger total area for building services.

For the UH models, adding openings generally reduces the strength retention ratio because more web material is removed and more regions are available for local deformation to develop. In the selected C290 models, Mu/M0 decreases from 0.8958 for one opening to 0.8848 for two openings and 0.8231 for three openings. The greater reduction for the three-hole model indicates that the combined effect of the removed web area and interaction between opening regions becomes more important as the number of openings increases.

The C240 UH models do not show a completely monotonic trend. Mu/M0 is 0.8509 for one opening, 0.8777 for two openings, and 0.8271 for three openings. The slightly higher value for the two-hole model demonstrates that the number of openings is not the only parameter controlling the response. The longitudinal positions of the openings, interaction between local deformation regions, and the governing buckling response may also affect the predicted capacity. Nevertheless, the three-hole model gives the lowest retention ratio among the selected C240 cases.

The EH models show a different response. For the C290 EH models, Mu/M0 is 1.0025 for one opening, 1.0328 for two openings, and 1.0284 for three openings. The values remain close to or slightly above the no-hole reference capacity even though the opening ratio increases. This indicates that the stiffened hole boundaries compensate for a substantial proportion of the local stiffness lost through the removal of web material.

The C290 values above 1.0 should not be interpreted as evidence that adding holes inherently improves beam strength. Within the analysed FE range, the edge stiffeners modify the local stiffness, stress distribution, and buckling response around the openings. This produces predicted capacities slightly higher than that of the no-hole reference model for some configurations.

For the C240 EH models, Mu/M0 is 0.9901 for one opening, 0.9822 for two openings, and 0.9812 for three openings. These values remain close to the no-hole capacity and are substantially higher than the corresponding UH values. However, the strength recovery is less pronounced than that obtained for the C290 EH models. This indicates that the effectiveness of edge stiffening also depends on the section geometry and slenderness.

Overall, increasing the number of openings increases the available service area but also increases the total disturbed region of the web. The UH models generally experience a greater capacity reduction as the number of openings increases. In comparison, the EH models retain a much larger proportion of the no-hole capacity because the stiffened boundaries restrain local deformation and improve stress transfer around the openings. However, the results are not strictly monotonic, and the number of openings should be considered together with the opening geometry, spacing, and section size.

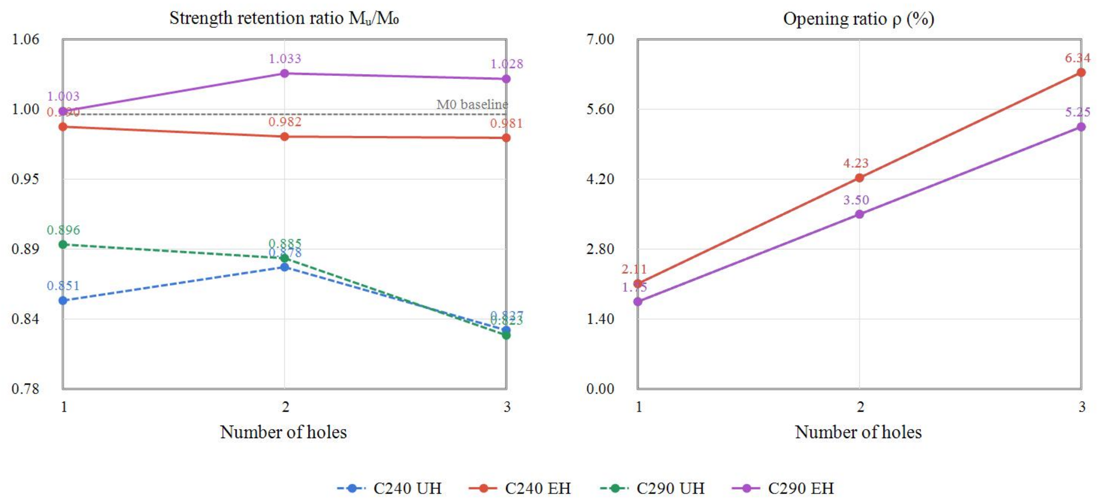

Figure 18 Effect of number of web holes on strength retention ratio and opening ratio.

4.8. Effect of lip angle

The influence of lip angle was examined using selected single-hole models with R = 80 mm and a/b = 1.5. The study included the C240 and C290 sections, with one UH1 series and one EH1 series considered for each section. Lip angles of 20, 45, 60, 75, and 90 degrees were investigated.

This investigation was included as an additional sensitivity study because lip angle was not considered as a separate parameter by Chen et al. [22]. Changing the lip angle modifies the orientation of the flange-lip junction and may influence the local stiffness of the section, flange rotation, and the interaction between the flange, web, and lip during bending. However, the present assessment is limited to the selected R80-a/b1.5 single-hole models.

As shown in Fig. 19, the selected UH1 models exhibit relatively small variations in strength retention with lip angle. For the C240 UH1 series, Mu/M0 is 0.837 at 20 degrees and 0.834 at 90 degrees, with only limited variation between the investigated angles. The selected C290 UH1 series shows a slightly greater variation. Mu/M0 increases from 0.851 at 20 degrees to 0.865 at 60 degrees and then decreases to 0.840 at 90 degrees.

These results indicate that lip angle has a limited influence on the peak moment capacity of the selected UH1 models. In these cases, the reduction associated with the unstiffened opening appears to remain the dominant influence. However, this observation should not be extended to other opening geometries or multi-hole arrangements without additional analysis.

The selected EH1 models show a more noticeable sensitivity. For the C240 EH1 series, Mu/M0 increases from 0.929 at 20 degrees to approximately 0.947 at 45 and 60 degrees. It then decreases slightly at 75 degrees and reaches 0.906 at 90 degrees. For the C290 EH1 series, Mu/M0 increases from 1.029 at 20 degrees to 1.064 at 60 degrees, remains similar at 75 degrees with a value of 1.062, and decreases to 1.008 at 90 degrees.

Within these selected EH1 cases, the higher strength-retention values occur between 45 and 75 degrees, and the highest value is obtained for the C290 EH1 model with a 60-degree lip. This response may be associated with a change in local section stiffness and restraint against flange rotation. Nevertheless, the present results do not directly demonstrate a change in local or distortional buckling mode, and further deformation or buckling-mode comparisons would be required to confirm the mechanism.

The C290 EH1 values above 1.0 should not be interpreted as evidence that the opening or inclined lip generally improves beam strength. Within the selected FE models, the combination of the inclined lip and edge-stiffened opening modifies the local stiffness and predicted buckling response, resulting in a capacity slightly higher than that of the no-hole reference model.

The present comparison is based only on selected C240 and C290 single-hole UH1 and EH1 models with R = 80 mm and a/b = 1.5. It does not include two-hole or three-hole arrangements, other radii, other aspect ratios, or different clear spacings. In addition, Fig. 4.7 compares peak strength retention and does not establish whether lip angle improves post-peak stability or ductility.

Therefore, the results should be interpreted as a limited sensitivity assessment. They indicate that lip angle has little influence on the selected UH1 models and a more noticeable influence on the selected EH1 models. However, the available dataset is insufficient to identify a generally optimal lip angle or to propose a design recommendation. A broader parametric and experimental investigation would be required before such conclusions could be established.

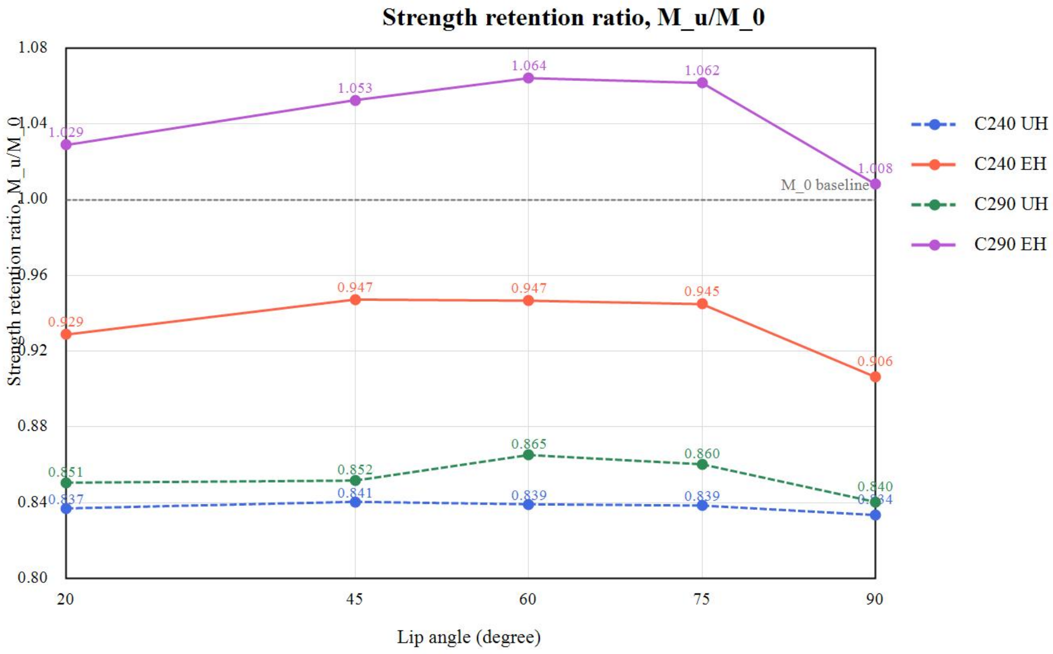

Figure 19 Effect of lip angle on the strength retention ratio of selected C240 and C290 R80-ab1.5 single-hole UH1 and EH1 models.

4.9. Practical evaluation of opening area and strength retention

In practical design, web openings must provide sufficient space for building services without causing an unacceptable loss of structural capacity. Increasing the size of an elongated opening provides more usable space but also removes more web material and may increase local deformation. Previous studies under bending and shear have similarly identified opening dimensions as important parameters affecting the capacity of cold-formed steel channels [34,37]. The present study therefore evaluates this practical trade-off using the opening ratio and strength retention ratio, Mu/M0.

Figure 20 presents the relationship between opening ratio and strength retention for the C290 models. The UH and EH results are shown separately, while different symbols represent models containing one, two, and three openings. The horizontal reference line at Mu/M0 = 1.0 represents the moment capacity of the corresponding no-hole model.

For the UH models, the strength retention ratio generally decreases as the opening ratio increases. The one-hole models occupy the lower opening-ratio range and generally retain a larger proportion of the no-hole capacity. The two-hole and three-hole models extend to larger opening ratios and mostly produce lower strength-retention values. This trend indicates that removing a greater proportion of the web increases deformation around the opening and reduces load transfer through the remaining web.

However, the UH results do not follow a single relationship with opening ratio. Models with similar opening ratios can have different strength-retention values. The scatter is particularly evident when the one-hole, two-hole, and three-hole groups are compared. This demonstrates that opening ratio is an important indicator but is not the only parameter controlling moment capacity. The opening aspect ratio, hole radius, number of openings, clear spacing, and section geometry also affect the structural response.

The EH models generally retain a greater proportion of the no-hole capacity than the UH models. Most of the C290 two-hole and three-hole EH results remain close to Mu/M0 = 1.0, even at relatively large opening ratios. This indicates that the edge stiffener can compensate for a substantial part of the local stiffness lost through the removal of web material. The stiffened hole boundary restrains deformation around the opening and promotes stress redistribution into the surrounding web and flanges.

Some EH models produce Mu/M0 values slightly greater than 1.0. These results should not be interpreted as evidence that web openings inherently increase beam strength. Within the analysed FE model range, the edge stiffener locally modifies the stiffness and buckling response around the opening. This can result in a predicted capacity that is slightly higher than that of the no-hole reference model. These values remain dependent on the adopted geometry, material model, imperfections, and boundary conditions.

The isolated lower values in both the UH and EH results further demonstrate that opening ratio alone cannot identify a suitable opening arrangement. A model with a moderate opening ratio may still perform poorly if its opening geometry produces an unfavourable local response. Conversely, a model with a relatively large opening ratio may retain a high moment capacity when an effective edge stiffener is provided. Opening ratio should therefore be considered together with the opening geometry and stiffening details.

The C240 results show the same general tendency, although the strength recovery provided by edge stiffening is less consistent than in the selected C290 models. This suggests that the effectiveness of edge stiffening also depends on the section dimensions and slenderness. Consequently, the C290 results should not be applied directly to other section sizes without further verification.

From a practical perspective, EH arrangements provide a more favourable balance between service-opening area and moment capacity than comparable UH arrangements. Nevertheless, the present results do not establish a universal maximum opening ratio or a general design rule. The conclusions are limited to the section sizes, opening geometries, material properties, loading arrangement, and FE assumptions examined in this study. Further experimental validation and a broader parametric range would be required before specific design limits could be proposed.

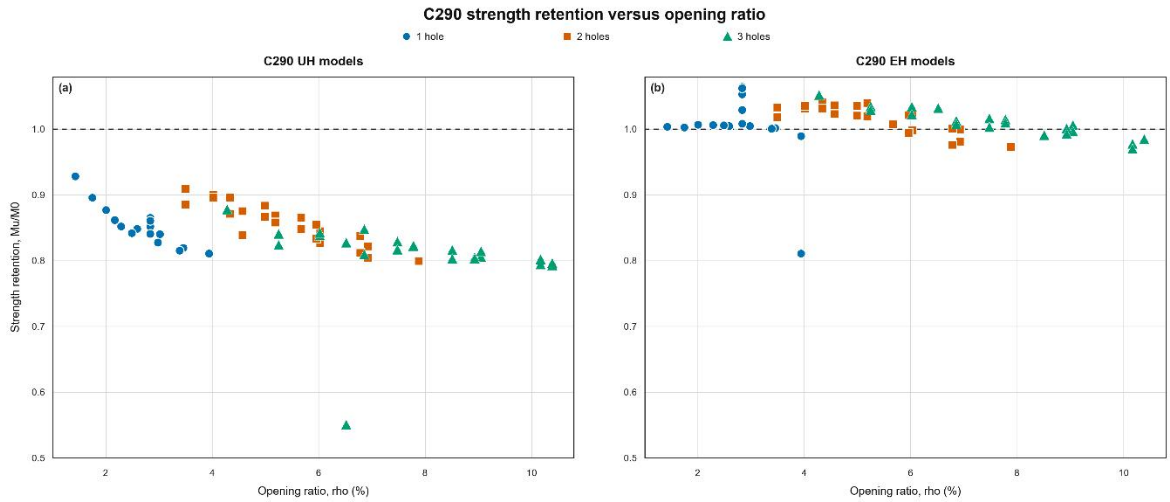

Figure 20 Relationship between strength retention and opening ratio for the C290 UH and EH models with one, two, and three elongated web openings.

5. Conclusions

5.1. Conclusions

This study investigated the flexural behaviour of cold-formed steel C-channel beams containing unstiffened and edge-stiffened elongated web holes under four-point bending. The FE modelling procedure was reproduced using the numerical results reported by Chen et al. [22], with predicted-to-reference moment-capacity ratios ranging from 0.960 to 1.042. A parametric study comprising 282 FE models was subsequently conducted to examine the effects of hole radius, elongated-hole aspect ratio, clear spacing, number of holes and lip angle.

The results showed that unstiffened elongated holes generally reduced moment capacity as the opening area increased. This reduction was associated with the removal of web material and the localisation of deformation around the openings. Edge stiffening generally improved both peak resistance and post-peak strength retention compared with equivalent unstiffened openings. The numerical deformation patterns suggest that the stiffened hole edge provided additional local restraint and modified the development of local buckling. However, its effectiveness depended on the combined effects of opening geometry, hole arrangement and section proportions.

Hole radius and aspect ratio affected not only ultimate moment capacity but also post-peak behaviour. Some models with larger openings achieved peak capacities close to those of smaller-opening models but experienced a more rapid post-peak reduction. The influence of clear spacing was not monotonic, demonstrating that spacing cannot be considered independently of hole radius, aspect ratio and number of holes. The selected lip-angle models also showed that lip geometry may alter the response of edge-stiffened openings, although the limited number of cases does not support identification of a generally optimum lip angle.

Some edge-stiffened models produced strength-retention ratios close to or slightly greater than unity. These results should not be interpreted as evidence that introducing web openings generally increases beam strength. Instead, within the analysed FE range, edge stiffening altered the local stiffness distribution and buckling response sufficiently for the predicted resistance to approach or marginally exceed that of the corresponding no-hole model. The results therefore provide comparative numerical trends rather than code-calibrated resistance limits.

Overall, the FE parametric results demonstrate the potential of edge stiffening to reduce the adverse effects of elongated web holes while permitting larger service openings. Nevertheless, the findings should not be used directly as final design rules. Future work should include experimental testing of representative elongated-hole beams, broader validation of failure and post-peak responses, more extensive imperfection sensitivity studies, additional section and lip-angle configurations, and investigation of edge-stiffener geometry. Statistical reliability analysis and calibration against appropriate safety targets would also be required before design equations or formal design recommendations could be developed.

5.2. Limitations

The findings of this study should be interpreted in consideration of the following limitations.

1. No experimental tests were conducted. The FE modelling procedure was reproduced using the results reported by Chen et al. [22], but the newly developed elongated-hole configurations were not directly tested. Therefore, their predicted strength, deformation and post-peak behaviour remain numerical results rather than direct experimental evidence.
2. Validation of the elongated-hole models was limited. The agreement with the reference results supports the general modelling procedure, but it does not fully validate every combination of hole radius, aspect ratio, spacing, number of holes and edge-stiffener geometry considered in the parametric study.
3. Mesh sensitivity study was not carried out for all models. The mesh arrangement was adopted mainly from Chen et al. [22], and selected reproduced models were checked against the published FE results. Therefore, the possible influence of mesh size on local stress concentration, buckling behaviour, and post-peak response should be recognised as a limitation of the present study.
4. Initial geometric imperfections were introduced using scaled eigenvalue buckling modes rather than measured geometries for individual specimens. The local buckling shape was obtained using an artificially reduced shell thickness, while selected eigenmodes were used to represent the local and global components. Distortional imperfections were not introduced separately in the main parametric models. Moreover, where corresponding measured data were unavailable for two-hole models, amplitudes from comparable three-hole specimens were adopted. These assumptions may affect the predicted buckling and post-peak responses.
5. Only the C240 and C290 channel sections were studied. Consequently, the observed trends may not apply directly to sections with substantially different web slenderness, flange width, lip length, thickness or material properties.
6. All models used the same beam length and four-point bending arrangement. The effects of span, shear-span ratio, moment gradient and alternative support or loading conditions were not examined.
7. The edge-stiffener length and fillet radius were fixed in most of the parametric models. The study therefore evaluated the selected stiffener configuration but did not establish an optimum edge-stiffener geometry.
8. The lip-angle investigation was restricted to selected R80-ab1.5 single-hole models. The apparent benefit of a moderate lip angle cannot be generalised to other hole dimensions, multiple-hole arrangements or channel sections without further analysis.
9. The investigation focused primarily on ultimate moment capacity, strength retention and moment-displacement behaviour. Residual stresses, fabrication tolerances, forming effects, serviceability limits, repeated loading and connection behaviour were not investigated in detail.
10. No statistical reliability analysis or safety-factor calibration was conducted. Accordingly, the strength-retention ratios and stiffening efficiencies obtained from the FE models are comparative numerical indices and should not be treated as final design limits or directly adopted as design rules.

5.3. Recommendations for future work

Future research should first include four-point bending tests on representative beams with unstiffened and edge-stiffened elongated web holes. The experimental programme should cover different opening sizes and multiple-hole arrangements, particularly configurations for which the present FE models predicted strength-retention ratios close to or slightly greater than unity. Measurements of load-displacement response, strains, initial imperfections and failure modes would provide direct validation of the numerical predictions.

The validation database should be expanded beyond the reference models adopted in this study. Comparisons should include ultimate moment capacity, initial stiffness, post-peak response, deformation patterns and stress or strain distributions around the openings. This would clarify whether the predicted benefits of edge stiffening are consistently reproduced in physical specimens.

Further imperfection sensitivity studies should examine local, distortional and global imperfections both separately and in combination. Different eigenmodes, amplitudes and signs should be considered, and the numerical imperfections should be compared with measured geometric imperfections where possible. This would reduce the uncertainty associated with the imperfection assumptions adopted in the present models.

A wider parametric range should also be studied. This should include additional channel dimensions and thicknesses, beam spans, shear-span ratios, hole arrangements, edge-stiffener lengths, fillet radii and lip angles. In particular, the lip-angle investigation should be extended beyond the selected R80-ab1.5 single-hole models before an optimum range is proposed.

Future studies should give greater attention to post-peak behaviour and serviceability. Appropriate indices could be developed to quantify post-peak strength retention, deformation capacity and stiffness degradation. The effects of residual stresses, fabrication tolerances, repeated loading, connections and practical forming requirements should also be investigated.

Finally, the combined experimental and numerical database could be used to develop preliminary design expressions for beams with elongated web holes. Such expressions should be subjected to statistical evaluation, reliability analysis and calibration against appropriate safety targets. Only after sufficient validation and reliability assessment should the numerical trends identified in this study be developed into formal design recommendations or final design rules.

6. References

[1] Howick Ltd. *Howick Floor Joist System*. 2013.

[2] Yu C, Schafer BW. Distortional buckling tests on cold-formed steel beams. *Journal of Structural Engineering*. 2006;132(4):515-528.

[3] Yu C, Schafer BW. Simulation of cold-formed steel beams in local and distortional buckling with applications to the direct strength method. *Journal of Constructional Steel Research*. 2007;63(5):581-590.

[4] Yu C, Yan W. Effective Width Method for determining distortional buckling strength of cold-formed steel flexural C and Z sections. *Thin-Walled Structures*. 2011;49:233-238.

[5] Wang L, Young B. Design of cold-formed steel channels with stiffened webs subjected to bending. *Thin-Walled Structures*. 2014;85:81-92.

[6] Anbarasu M. Local-distortional buckling interaction on cold-formed steel lipped channel beams. *Thin-Walled Structures*. 2016;98:351-359.

[7] Zhao J, Sun K, Yu C, Wang J. Tests and direct strength design on cold-formed steel channel beams with web holes. *Engineering Structures*. 2019;184:434-446.

[8] Moen CD. *Direct Strength Design of Cold-Formed Steel Members with Perforations*. PhD thesis. Johns Hopkins University; 2008.

[9] Moen CD, Schafer BW. Elastic buckling of cold-formed steel columns and beams with holes. *Engineering Structures*. 2009;31:2812-2824.

[10] Moen CD, Schudlich A, Heyden A. Experiments on cold-formed steel C-section joists with unstiffened web holes. *Journal of Structural Engineering*. 2013;139(5):695-704.

[11] Yu NT, Kim B, Yuan WB, Li LY, Yu F. An analytical solution of distortional buckling resistance of cold-formed steel channel-section beams with web openings. *Thin-Walled Structures*. 2019;135:446-452.

[12] Yu NT, Kim B, Li LY, Hong WJ, Yuan WB. Distortional buckling of perforated cold-formed steel beams subject to uniformly distributed transverse loads. *Thin-Walled Structures*. 2020;148:106569.

[13] Kulatunga MP, Macdonald M. Investigation of cold-formed steel structural members with perforations of different arrangements subjected to compression loading. *Thin-Walled Structures*. 2013;67:78-87.

[14] Kulatunga MP, Macdonald M, Rhodes J, Harrison DK. Load capacity of cold-formed column members of lipped channel cross-section with perforations subjected to compression loading - Part I: FE simulation and test results. *Thin-Walled Structures*. 2014;80:1-12.

[15] Chen B, Roy K, Uzzaman A, Raftery GM, Nash D, Clifton GC, Pouladi P, Lim JBP. Effects of edge-stiffened web openings on the behaviour of cold-formed steel channel sections under compression. *Thin-Walled Structures*. 2019;144:106307.

[16] Chen B, Roy K, Uzzaman A, Raftery GM, Lim JBP. Parametric study and simplified design equations for cold-formed steel channels with edge-stiffened holes under axial compression. *Journal of Constructional Steel Research*. 2020;172:106161.

[17] Yu C. Cold-formed steel flexural member with edge stiffened web openings: behavior, optimization, and design. *Journal of Constructional Steel Research*. 2012;71:210-218.

[18] Uzzaman A, Lim JBP, Nash D, Young B. Effects of edge-stiffened circular web openings on the web crippling strength of cold-formed steel channel beams under one-flange loading conditions. *Engineering Structures*. 2017;139:96-107.

[19] Uzzaman A, Lim JBP, Nash D, Roy K. Cold-formed steel channel beams under end-two-flange loading condition: design for edge-stiffened holes, unstiffened holes and plain webs. *Thin-Walled Structures*. 2020;147:106532.

[20] American Iron and Steel Institute. *North American Specification for the Design of Cold-Formed Steel Structural Members, AISI S100-16*. Washington, DC: AISI; 2016.

[21] Standards Australia/Standards New Zealand. *Cold-Formed Steel Structures, AS/NZS 4600:2018*. Sydney/Wellington: Standards Australia/Standards New Zealand; 2018.

[22] Chen B, Roy K, Uzzaman A, Lim JBP. Moment capacity of cold-formed channel beams with edge-stiffened web holes, un-stiffened web holes and plain webs. Thin-Walled Structures. 2020.

[23] Dassault Systèmes. Abaqus Analysis User's Manual, Version 2024. Dassault Systèmes Simulia Corp., Providence, RI, USA; 2024.

[24] Schafer BW, Peköz T. Computational modeling of cold-formed steel: characterizing geometric imperfections and residual stresses. Journal of Constructional Steel Research. 1998;47(3):193–210.

[25] Lim JBP, Nethercot DA. Finite element idealization of a cold-formed steel portal frame. Journal of Structural Engineering. 2004;130(1):78–94.

[26] Keerthan P, Mahendran M. Numerical studies of lean duplex stainless steel beams. Journal of Constructional Steel Research. 2014;100:1–12.

[27] Ellobody E, Young B. Behavior of cold-formed steel plain angle columns. Journal of Structural Engineering. 2005;131(3):457–466.

[28] Ye, J., Mojtabaei, S. M., Hajirasouliha, I., Shepherd, P., & Pilakoutas, K. (2019). Experimental investigation of cross-sectional bending capacity of cold-formed steel channels subject to local-distortional buckling interaction. Journal of Structural Engineering, 145(7), 04019064.

[29] Dassault Systèmes. (2024). Abaqus 2024 documentation. SIMULIA user assistance. https://www.3ds.com/support/documentation/user-guides

[30] Feng, R., Zhan, H., Meng, S., & Zhu, J. (2018). Experiments on H-shaped high-strength steel beams with perforated web. Engineering Structures, 177, 374-394.

[31] Feng, R., Shen, C., & Lin, J. (2019). Finite-element analysis and design of aluminium alloy CHSs with circular through-holes in bending. Thin-Walled Structures, 144, 106289.

[32] Young, B., & Ellobody, E. (2005). Buckling analysis of cold-formed steel lipped angle columns. Journal of Structural Engineering, 131(10), 1570-1579.

[33] LaBoube, R. A., Yu, W.-W., Langan, J. E., & Shan, M. Y. (1997). Cold-formed steel webs with openings: Summary report. *Thin-Walled Structures, 27*(1), 79-84.

[34] Chandramohan, D. L., Roy, K., Fang, Z., Ananthi, G. B. G., & Lim, J. B. P. (2025). Moment capacity of cold-formed steel channel beams with edge-stiffened and unstiffened elongated web holes. *Thin-Walled Structures, 206*, 112605.

[35] Chandramohan, D. L., Roy, K., Fang, Z., Ananthi, G. B. G., & Lim, J. B. P. (2024). Numerical investigation of cold-formed steel channels with edge-stiffened and unstiffened elongated web holes under shear. *Thin-Walled Structures, 196*, 111472.

[36] Chandramohan, D. L., Roy, K., Ananthi, G. B. G., Fang, Z., & Lim, J. B. P. (2024). Structural behaviour and capacity of cold-formed steel channel sections with elongated edge-stiffened and unstiffened web holes under compression. *Journal of Constructional Steel Research, 218*, 108681.

[37] Pham, D. K., Pham, C. H., & Hancock, G. J. (2020). Parametric study for shear design of cold-formed channels with elongated web openings. *Journal of Constructional Steel Research, 172*, 106222.